

2

NAVAL POSTGRADUATE SCHOOL
Monterey, California

AD-A275 050



DTIC
ELECTE
JAN 27 1994
S E D

THESIS

**AN ANALYSIS OF THE MICROSTRUCTURE AND
REINFORCEMENT DISTRIBUTION OF AN EXTRUDED
PARTICLE-REINFORCED AL 6061-10 VOLUME PERCENT
Al₂O₃ METAL MATRIX COMPOSITE**

by

Fredric W. Longenecker

September 1993

Thesis Advisor:

Terry R. McNelley

Approved for public release; distribution is unlimited.

94-02740



94 1 26 186

Unclassified

Security Classification of this page

REPORT DOCUMENTATION PAGE

1a Report Security Classification: Unclassified			1b Restrictive Markings		
2a Security Classification Authority			3 Distribution/Availability of Report		
2b Declassification/Downgrading Schedule			Approved for public release; distribution is unlimited.		
4 Performing Organization Report Number(s)			5 Monitoring Organization Report Number(s)		
6a Name of Performing Organization Naval Postgraduate School		6b Office Symbol (if applicable) *34	7a Name of Monitoring Organization Naval Postgraduate School		
6c Address (city, state, and ZIP code) Monterey CA 93943-5100			7b Address (city, state, and ZIP code) Monterey CA 93943-5100		
8a Name of Funding/Sponsoring Organization		6b Office Symbol (if applicable)	9 Procurement Instrument Identification Number		
Address (city, state, and ZIP code)			10 Source of Funding Numbers		
			Program Element No	Project No	Task No
			Work Unit Accession No		
11 Title (include security classification) *An Analysis of the Microstructure and Reinforcement Distribution for an Extruded Particle-Reinforced Al 6061-10 Volume Percent Al ₂ O ₃ Metal Matrix Composite					
12 Personal Author(s) *Fredric W. Longenecker					
13a Type of Report Master's Thesis		13b Time Covered From To	14 Date of Report (year, month, day) *September 1993	15 Page Count * 81	
16 Supplementary Notation The views expressed in this thesis are those of the author and do not reflect the official policy or position of the Department of Defense or the U.S. Government.					
17 Cosati Codes			18 Subject Terms (continue on reverse if necessary and identify by block number)		
Field	Group	Subgroup	*Extruded Particle-Reinforced MMC, Matrix Metal Microstructure, Reinforcement Particle Distribution Throughout the Matrix Metal		
19 Abstract					
<p>This research was performed in conjunction with funding by DURALCAN-USA through a Cooperative Research and Development Agreement (CRDA). The program seeks to improve the ductility of cast and extruded Al 6061-Al₂O₃ metal matrix composite (MMC) materials. Annealing stages were designed to be introduced into combined extrusion and drawing operations during the processing of the MMCs. This work has included a comprehensive analysis of a composite's microstructure as related to processing strains ranging from zero to 5.32 during extrusion/drawing operations. As the strains were increased, particle clusters present in the as-cast material were dispersed and the particle distribution became more uniform. Strains of greater than 4.0 were required in order to disperse the clusters and substantially eliminate banding of the particle distribution. The recrystallized grain size in the Al matrix decreased as increased processing strain was applied to the material. The grain size appeared to be stable and resistant to coarsening during subsequent solution heat treatment. Quantitative image analysis revealed no change in apparent particle size or aspect ratio indicating no fracturing of the particles during processing. The image analysis revealed no readily measurable feature to be used to assess uniformity of the particle distribution.</p>					
20 Distribution/Availability of Abstract _X unclassified/unlimited _ same as report _ DTIC users			21 Abstract Security Classification Unclassified		
22a Name of Responsible Individual *T. R. McNelley			22b Telephone (include Area Code) *(408) 646-2589	22c Office Symbol *ME/Mc	

DD FORM 1473,84 MAR

83 APR edition may be used until exhausted

All other editions are obsolete

security classification of this page

Unclassified

Approved for public release; distribution is unlimited.

An Analysis of the Microstructure and Reinforcement
Distribution of an Extruded Particle-Reinforced Al 6061-10 Volume
Percent Al₂O₃ Metal Matrix Composite

by

Fredric W. Longenecker
Lieutenant, United States Navy
B.S., The Pennsylvania State University, 1983

Submitted in partial fulfillment
of the requirements for the degree of

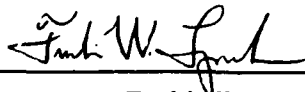
MASTER OF SCIENCE IN MECHANICAL ENGINEERING

from the

NAVAL POSTGRADUATE SCHOOL

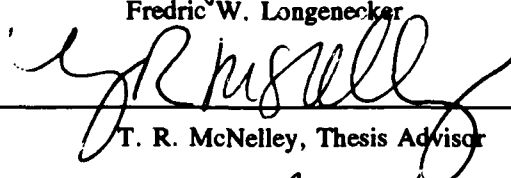
September 1993

Author:



Fredric W. Longenecker

Approved by:



T. R. McNelley, Thesis Advisor



Matthew D. Kelleher, Chairman
Department of Mechanical Engineering

Accession For	
NTIS	CRA&I <input checked="" type="checkbox"/>
DTIC	TAB <input type="checkbox"/>
Unannounced <input type="checkbox"/>	
Justification	
By	
Distribution /	
Availability Codes	
Dist	Avail and/or Special
A-1	

ABSTRACT

This research was performed in conjunction with funding by DURALCAN-USA through a Cooperative Research and Development Agreement (CRDA). The program seeks to improve the ductility of cast and extruded Al 6061-Al₂O₃ metal matrix composite (MMC) materials. Annealing stages were designed to be introduced into combined extrusion and drawing operations during the processing of the MMCs. This work has included a comprehensive analysis of a composite's microstructure as related to processing strains ranging from zero to 5.32 during extrusion/drawing operations. As the strains were increased, particle clusters present in the as-cast material were dispersed and the particle distribution became more uniform. Strains of greater than 4.0 were required in order to disperse the clusters and substantially eliminate banding of the particle distribution. The recrystallized grain size in the Al matrix decreased as increased processing strain was applied to the material. The grain size appeared to be stable and resistant to coarsening during subsequent solution heat treatment. Quantitative image analysis revealed no change in apparent particle size or aspect ratio indicating no fracturing of the particles during processing. The image analysis revealed no readily measurable feature to be used to assess uniformity of the particle distribution.

TABLE OF CONTENTS

I. INTRODUCTION	1
II. BACKGROUND	3
III. EXPERIMENTAL PROCEDURE	9
A. MATERIALS AND SECTIONING	9
B. DESIGN AND MACHINING OF TENSILE SPECIMEN	11
C. HEAT TREATING	14
D. AGING STUDY	15
E. MECHANICAL TESTING (HARDNESS AND TENSILE)	16
F. POLISHING SCHEDULE AND ANODIZATION	16
G. OPTICAL MICROSCOPY	18
H. IMAGE ANALYSIS	19
IV. RESULTS	21
A. THE EFFECT OF PROCESSING STRAIN ON PARTICLE DISTRIBUTION	21
1. Visual Interpretation of The Microstructure	21
2. Computational Analysis of Photomicrographs .	25
B. THE EFFECT OF PROCESSING STRAIN ON MATRIX GRAIN STRUCTURE	34
1. Influence of Processing Strain	34

2. The Effect of Solution Treatment	39
C. HARDNESS MEASUREMENTS OF UNREINFORCED 6061 AL AND A 10 V/O MMC	43
D. TENSILE TESTING OF EXTRUDED UNREINFORCED 6061 ALUMINUM	46
V. CONCLUSIONS	49
VI. RECOMMENDATIONS FOR FURTHER STUDY	50
APPENDIX A	51
APPENDIX B	54
LIST OF REFERENCES	65
INITIAL DISTRIBUTION LIST	68

LIST OF TABLES

TABLE I:	POLISHING SCHEDULE.	17
TABLE II:	FIRST NEAREST NEIGHBOR DISTANCES ASPECT RATIOS, MAXIMUM PARTICLE DIAMETER, AND AVERAGE PARTICLE DIAMETER FOR VARIOUS PROCESSING CONDITIONS SHOWN IN FIGURE 1.	28
TABLE III:	MEAN NEAREST NEIGHBOR DISTANCES (CALCULATED AND OBSERVED).	31
TABLE IV:	MATRIX GRAIN SIZES FOR VARIOUS TOTAL PROCESSING STRAINS.	38
TABLE V:	THE EFFECT OF SOLUTIONIZATION TEMPERATURE ON MATRIX GRAIN SIZE.	42

LIST OF FIGURES

Figure 1(a):	Computer Generated Random Distribution of Points and Particles with a Lognormal Size Distribution.	5
Figure 1(b):	Size Distribution Plot for the Random Distribution of Particles shown in Figure 1(a).	6
Figure 2:	Processing Schedule for the Al 6061-Al ₂ O ₃ Metal Matrix Composite.	10
Figure 3:	0.5 Inch (12.7 mm) Tensile Test Buttonhead Design.	12
Figure 4(a):	0.375 Inch (9.5 mm) Tensile Test Buttonhead Design.	13
Figure 4(b):	Insert Design for 0.375 inch (9.5mm) Diameter Bar Tensile Testing.	13
Figure 5:	Optical Micrograph of As-Cast Condition for Al 6061 - 10 v/o Al ₂ O ₃ MMC.	22
Figure 6:	Optical Micrograph of Forged Condition for Al 6061 - 10 v/o Al ₂ O ₃ MMC.	22
Figure 7:	Optical Micrograph of Rolled Condition for Al 6061 - 10 v/o Al ₂ O ₃ MMC.	22
Figure 8:	Optical Micrograph of Single Extrusion to 2.5 inches (63.5mm) Diameter Bar.	23
Figure 9:	Optical Micrograph of Twice Extruded to 0.824 inches (20.9mm) Diameter Bar.	23
Figure 10:	Optical Micrograph of Twice Extruded to 0.642 inches (16.3mm) Diameter Bar.	24
Figure 11:	Optical Micrograph of Twice Extruded to 0.5 inches (12.7mm) Diameter Bar.	24
Figure 12(a):	Optical Micrograph of Single Extrusion to 2.5 inches (63.5mm) Diameter Bar.	26
Figure 12(b):	Optical Micrograph of Single Extrusion to 2.5 inches (63.5mm) Diameter Bar.	26
Figure 13(a):	Optical Micrograph of Twice Extruded to 0.5 inches (12.7mm) Diameter Bar.	27

Figure 13(b):	Optical Micrograph of Single Extruded to 0.5 inches (12.7mm) Diameter Bar.	27
Figure 14:	Plot of Mean Aspect Ratio vs. Total Processing Strain.	29
Figure 15:	Plot of Maximum Particle Diameter vs. Total Processing Strain.	29
Figure 16:	Plot of Mean Particle Diameter vs. Total Processing Strain.	29
Figure 17:	Plot of First Nearest Neighbor Distances vs. Total Processing Strain.	31
Figure 18(a):	Histogram of First Nearest Neighbor Distances for Micrograph shown in Figure 18(b).	33
	(b): Optical Micrograph Repeated from Figure 13(b).	33
Figure 19:	Anodized Photomicrograph of As-Cast Condition for a 6061-Al 10 v/o Al ₂ O ₃ MMC.	35
Figure 20:	Anodized Photomicrograph of a Single Extruded to 2.5 inches (63.5mm) Diameter Bar.	35
Figure 21 (a):	Anodized Photomicrograph of a Twice Extruded to 0.824 inches (20.9mm) Diameter Bar.	37
	(b): Anodized Photomicrograph of a Twice Extruded to 0.642 inches (16.3mm) Diameter Bar.	37
	(c): Anodized Photomicrograph of a Twice Extruded to 0.5 inches (12.7mm) Diameter Bar.	37
Figure 22:	Plot of Matrix Grain Size vs. Total Processing Strain.	38
Figure 23 (a):	Anodized Photomicrograph of a Twice Extruded to 0.5 inches (12.7mm) Diameter Bar.	39
	(b): Anodized Photomicrograph of a Twice Extruded to 0.5 inches (12.7mm) Diameter Bar.	40
	(c): Anodized Photomicrograph of a Twice Extruded to 0.5 inches (12.7mm) Diameter Bar.	40
	(d): Anodized Photomicrograph of a Twice Extruded to 0.5 inches (12.7mm) Diameter Bar.	41
	(e): Anodized Photomicrograph of a Twice Extruded to 0.5 inches (12.7mm) Diameter Bar.	41

Figure 24:	Hardness vs. Aging Time. (MMC vs. Unreinforced Al)	44
Figure 25:	Hardness vs. Aging Time. (Unreinforced Al) .	45
Figure 26:	Ultimate Tensile Strength vs. Aging Time. . .	47
Figure 27:	0.2% Yield Strength vs. Aging Time.	48
Figure 28:	Particle Aspect Ratio Distribution for 7 inch (177.8mm) Diameter Casting.	55
Figure 29:	Particle Aspect Ratio Distribution for the Forged Condition.	55
Figure 30:	Particle Aspect Ratio Distribution for the Forged Condition.	56
Figure 31:	Particle Aspect Ratio Distribution for the Once Extruded to 2.5 inch (63.5mm) Diameter Bar. .	56
Figure 32:	Particle Aspect Ratio Distribution for the Once Extruded to 2.5 inch (63.5mm) Diameter Bar. .	57
Figure 33:	Particle Aspect Ratio Distribution for the Twice Extruded to 0.824 inch (20.9mm) Diameter Bar.	57
Figure 34:	Particle Aspect Ratio Distribution for the Twice Extruded to 0.642 inch (16.3mm) Diameter Bar.	58
Figure 35:	Particle Aspect Ratio Distribution for the Twice Extruded to 0.5 inch (12.7mm) Diameter Bar.	58
Figure 36:	Particle Aspect Ratio Distribution for the Once Extruded to 0.5 inch (12.7mm) Diameter Bar. .	59
Figure 37:	Particle First Nearest Neighbor Distance Distribution for 7 inch (177.8mm) Diameter Casting.	60
Figure 38:	Particle First Nearest Neighbor Distance Distribution for the Forged Condition.	60
Figure 39:	Particle First Nearest Neighbor Distance Distribution for the Rolled Condition.	61
Figure 40:	Particle First Nearest Neighbor Distance Distribution for the Once Extruded to 2.5 inch (63.5mm) Diameter Bar.	61

Figure 41:	Particle First Nearest Neighbor Distance Distribution for the Once Extruded to 2.5 inch (63.5mm) Diameter Bar.	62
Figure 42:	Particle First Nearest Neighbor Distance Distribution for the Twice Extruded to 0.824 inch (20.9mm) Diameter Bar.	62
Figure 43:	Particle First Nearest Neighbor Distance Distribution for the Twice Extruded to 0.642 inch (16.3mm) Diameter Bar.	63
Figure 44:	Particle First Nearest Neighbor Distance Distribution for the Twice Extruded to 0.5 inch (12.7mm) Diameter Bar.	63
Figure 45:	Particle First Nearest Neighbor Distance Distribution for the Twice Extruded to 0.5 inch (12.7mm) Diameter Bar.	64

ACKNOWLEDGEMENTS

I would like to express my sincere thanks to Professors Terry McNelley and Roy Crooks for their guidance and assistance. I would also like to thank my wife Melody and son Jarret for their continued love and support throughout our time at the Naval Postgraduate School. Also, I would like to express thanks to Bill Dixon of DURALCAN for his assistance in supplying the composite material and providing technical support. Lastly, I would like to thank my fellow classmates Kurt, Peter, and Werner who collectively helped solve many procedural problems throughout the research.

I. INTRODUCTION

Engineers and designers are continually seeking materials which maximize desired characteristics and minimize unwanted detrimental traits. Composite materials, specifically particle-reinforced metal matrix composites (MMCs), have been developed to combine the positive attributes of both the metallic matrix and the reinforcement ceramic particles. The metal matrix is intended to provide strength and toughness while the ceramic reinforcement particles enhance stiffness, provide wear resistance and further strengthening as well [Ref. 1].

When compared to monolithic alloys, the positive traits of MMCs, such as higher strengths, higher stiffnesses, and greater resistance to wear, are recognized. The most negative aspect of MMC mechanical properties is low ductility and toughness. Advances in fabrication procedures [Ref. 2] and thermomechanical processing (TMP) methods [Ref 3] have demonstrated that the ductility problem can be alleviated. The current study was initiated to determine if the ductility of extruded MMC products can be improved by incorporating TMP modifications similar to those of previous work [Ref. 3].

Many of the desired mechanical properties of an MMC are dependent on both the size and distribution of the

reinforcement particles [Ref. 4]. Very fine particles may provide strengthening via the Orowan mechanism. The particles characteristic of the materials of interest here are much too large for strengthening in this manner. A complete theory of strength, deformation, and fracture in these materials has yet to be developed but must include effects of particles on the matrix microstructure and consider the homogeneity of the particle distribution.

Improved MMC ductility will expand applications of these materials and offer many advantages to both the military and civilian markets. Transporting people and/or supplies plays a large role in both the military and civilian sectors. If the various components which make up the vehicles can be made lighter, this savings could allow a heavier cargo to be carried or simply provide a savings in the fuel required to transport the material. Lighter weapon system components allow larger payloads or greater amounts of fuel to be carried, ultimately increasing the weapon system capabilities.

A specific civil application of an extruded MMC has been automotive drive shafts. In this application, the improved modulus to density ratio (E/ρ) results in improved component dynamic performance. Improved MMC ductility will further expand the range of such applications.

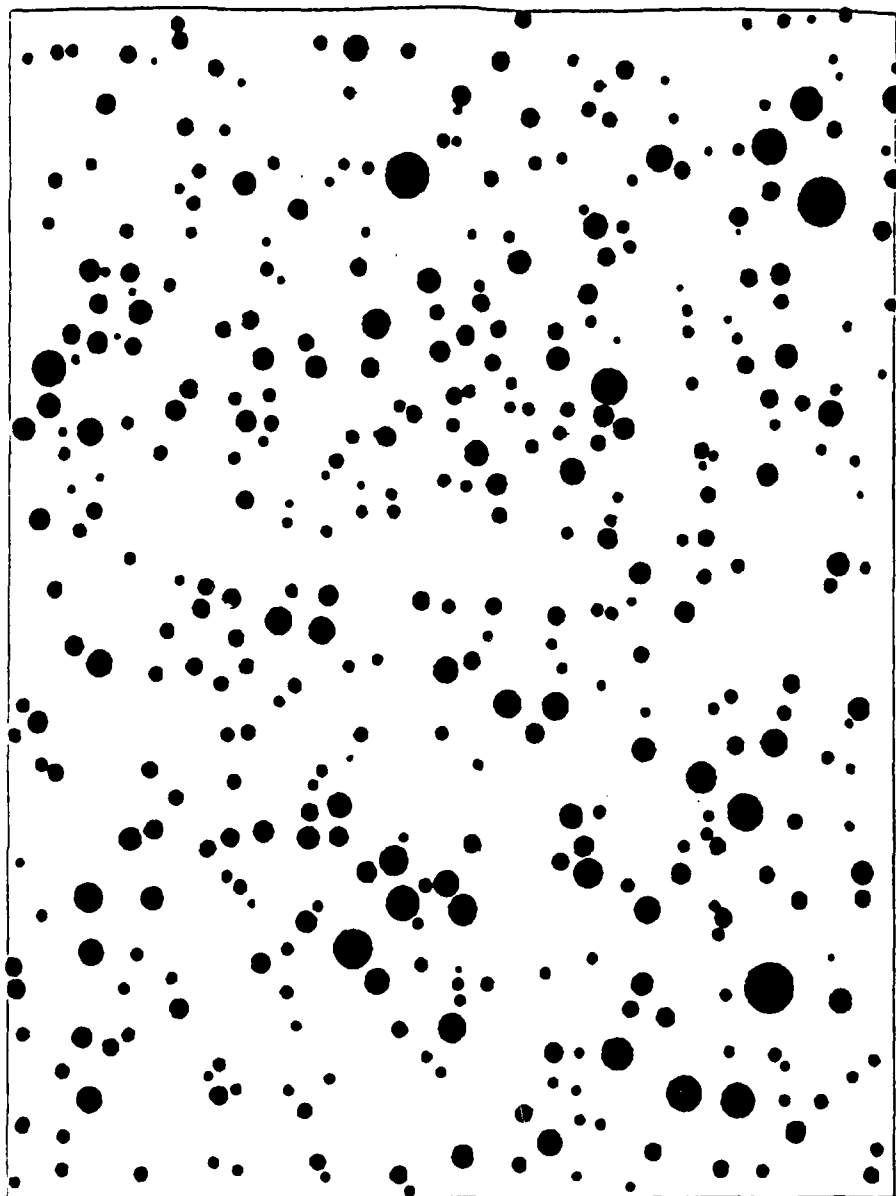
II. BACKGROUND

Previous research at the Naval Postgraduate School (NPS) has applied processing methods developed in study of superplastic aluminum to the ductility problems of particle reinforced MMCs. This work demonstrated the ability to increase a composite's ductility via TMP. These results prompted DURALCAN-USA to support application of these TMPs to existing industrial practices. DURALCAN has shown that extrusion of MMCs is a very competitive production avenue, with the major difference from extruding unreinforced aluminum being the higher rate of die wear [Ref. 5]. Initial research done at NPS analyzed the properties of a TMP'd 6061 Al-Al₂O₃ MMC. This material had already been extruded to a round-cornered rectangular bar with a total strain of $\epsilon_{\text{total}} = 2.83$. Additional TMP was conducted via a series of rolling and annealing stages. Improved ductility achieved through the additional TMP was associated with homogenization of the particle distribution and refinement of the matrix microstructure via particle-stimulated nucleation (PSN) of recrystallization. The present program has been structured to investigate the possibility of attaining similar property improvement by introducing drawing and annealing treatments into production of extruded MMC material.

Further details of previous MMC processing studies at NPS along with a general historical perspective on MMCs have been given previously [Refs. 6, 7, and 8]. A unique effort [Ref 9] was devoted to characterization of particle distributions by means of computer simulations. These computer simulations of particle distributions were done in two dimensions [Ref. 9]. Random distribution of particles having a lognormal size distribution were generated as shown in Figure 1 (a). Particle locations were determined using random number generators and accepted if the particle in question would not overlap any other previously sited particle. Once an array of particles has been generated, the distance from the i^{th} particle to all other particles was calculated using equation 1.

$$D_j = \sqrt{(X_i - X_j)^2 + (Y_i - Y_j)^2} \quad (i \neq j) \quad (1)$$

The distance to the nearest neighbor (NND) was found in turn for each of the particles in Figure 1 (a), [(X_i, Y_i) are the coordinates of the i^{th} particle's centroid and (X_j, Y_j) are the coordinates of all other particle centroids], by saving only the minimum value for each particle, i.e. NND = minimum value of D_j . Figure 1 (b) illustrates the size distribution plot for the number of particles vs. NND as they were located in Figure 1 (a).



PARTICLE AREA FRACTION: 0.10
MEAN PARTICLE RADIUS: 0.0503
AVERAGE NEAREST NEIGHBOR SPACING: 0.1808
NUMBER PARTICLES PER UNIT AREA: 10.75

Figure 1(a): Computer Generated Random Distribution of Points and Particles with a Lognormal Size Distribution (Reproduced from Ref. 9).

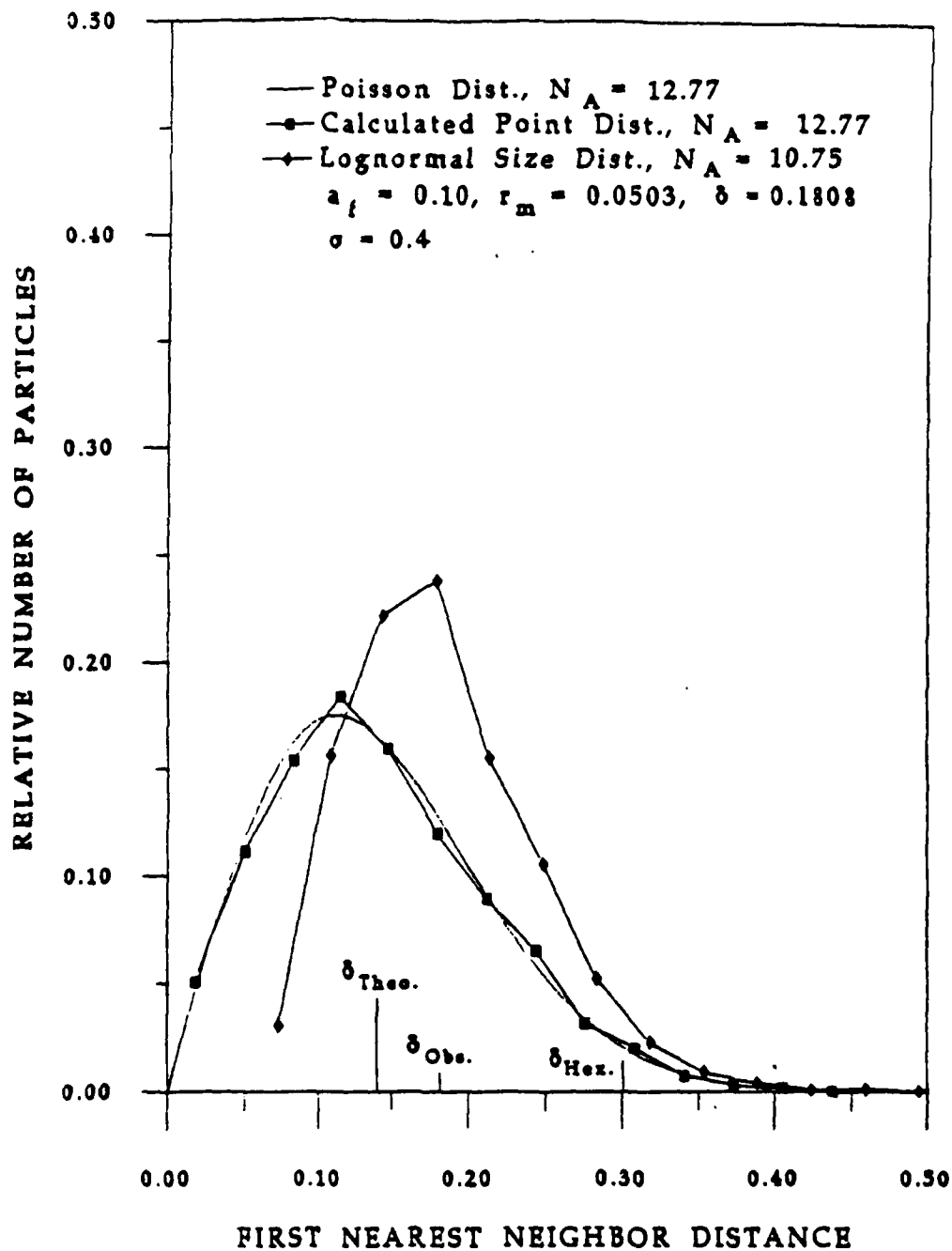


Figure 1(b): Size Distribution Plot for the Random Distribution of Particles shown in Figure 1(a) (Reproduced from Ref. 9).

The vertical line marked δ_{Theo} , on Figure 1 (b) was found using the equation

$$\delta_{\text{Theo}} = \frac{0.500}{\sqrt{N_A}} \quad (2)$$

where N_A is the number of particles per unit area, and δ_{Theo} was the mean value of NND for a random (Poisson) distribution of particles [Ref. 10]. The vertical line marked $\delta_{\text{Obs.}}$ was found by averaging all NNDs for a particular plot. The vertical line marked $\delta_{\text{Hex.}}$ was found using the equation,

$$\delta_{\text{Hex}} = \frac{1.075}{\sqrt{N_A}} \quad (3)$$

and was the mean value of NNDs for a regular hexagonal array. [Ref. 9]

In the study by Manfredi [Ref. 9], non-random distributions were generated by artificially creating bands of high particle concentration. One of the conclusions drawn in that work was that the human eye is the most effective differentiator between random and non-random particle distributions.

It is generally recognized that mechanical properties of MMCs can be adversely affected by non-uniform distributions of reinforcement particles. Thus, image analysis software was

employed to compute NND distribution distances for the MMC of interest and compare these determinations to Manfredi's simulation results [Ref. 9].

Previous work, both at NPS and elsewhere, has shown that the matrix grain size of an aluminum-based MMC may be refined by PSN of recrystallization. Following Humphreys, Basu, and Djazeb [Ref. 11], the matrix grain size for an Al_2O_3 particle size of 12 microns (the nominal size of the Al_2O_3 of interest here) should be given by the following equation:

$$D = d[(1 - F_v) / F_v]^{1/3} \quad (4)$$

where d = size of the reinforcement particle

F_v = volume fraction of the reinforcement

D = grain diameter.

An upper limit for the grain size, if boundary migration were limited by Zener drag, would obey:

$$D = (3d) / (2F_v) \quad (5)$$

with variables having the same definitions as in equation 4 above [Ref 12]. For a 10 volume percent (v/o) MMC containing 12 micron particles, equation 4 predicts a grain size of 25 microns and equation 5 predicts a size of 80 microns. In addition to evaluating the grain sizes of the extruded materials, an attempt will be made to assess the underlying mode of transformation for these materials.

III. EXPERIMENTAL PROCEDURE

A. MATERIALS AND SECTIONING

All of the MMC material for this research was provided by DURALCAN-USA of San Diego, California. Unreinforced 6061 Al bar was obtained from stock at NPS.

The processing schedules shown schematically in Figure 2 were used to produce the various extruded conditions of the MMC. Rolled materials were studied by Hoyt [Ref. 13]. Direct chill castings 7.0 inches (177.8 mm) in diameter and 20 inches (508 mm) in length provided the starting billets. From these billets, 2.5 inch (63.5 mm) diameter bars were extruded by Universal Alloy Inc., Anaheim, CA. Nominal extrusion temperature was 427-454° C and speed was 25-30 feet per minute (7.6 - 9.1 meters per minute). These bars were then cut into 10-inch (254 mm) lengths to allow for further extrusion. Three subsequent process paths were mapped to produce 0.5 inch (12.7 mm) diameter bar stock. The first was a direct extrusion from 2.5 inches (63.5 mm) to 0.5 inches (12.7 mm). The second produced a 0.642 inch (16.3 mm) diameter bar which was then drawn and annealed twice (each draw corresponded to a strain of 0.25) to provide the 0.5 inch (12.7 mm) diameter bar. The final path involved a 0.824 inch (20.9 mm) diameter bar which was then drawn and annealed four times with strains

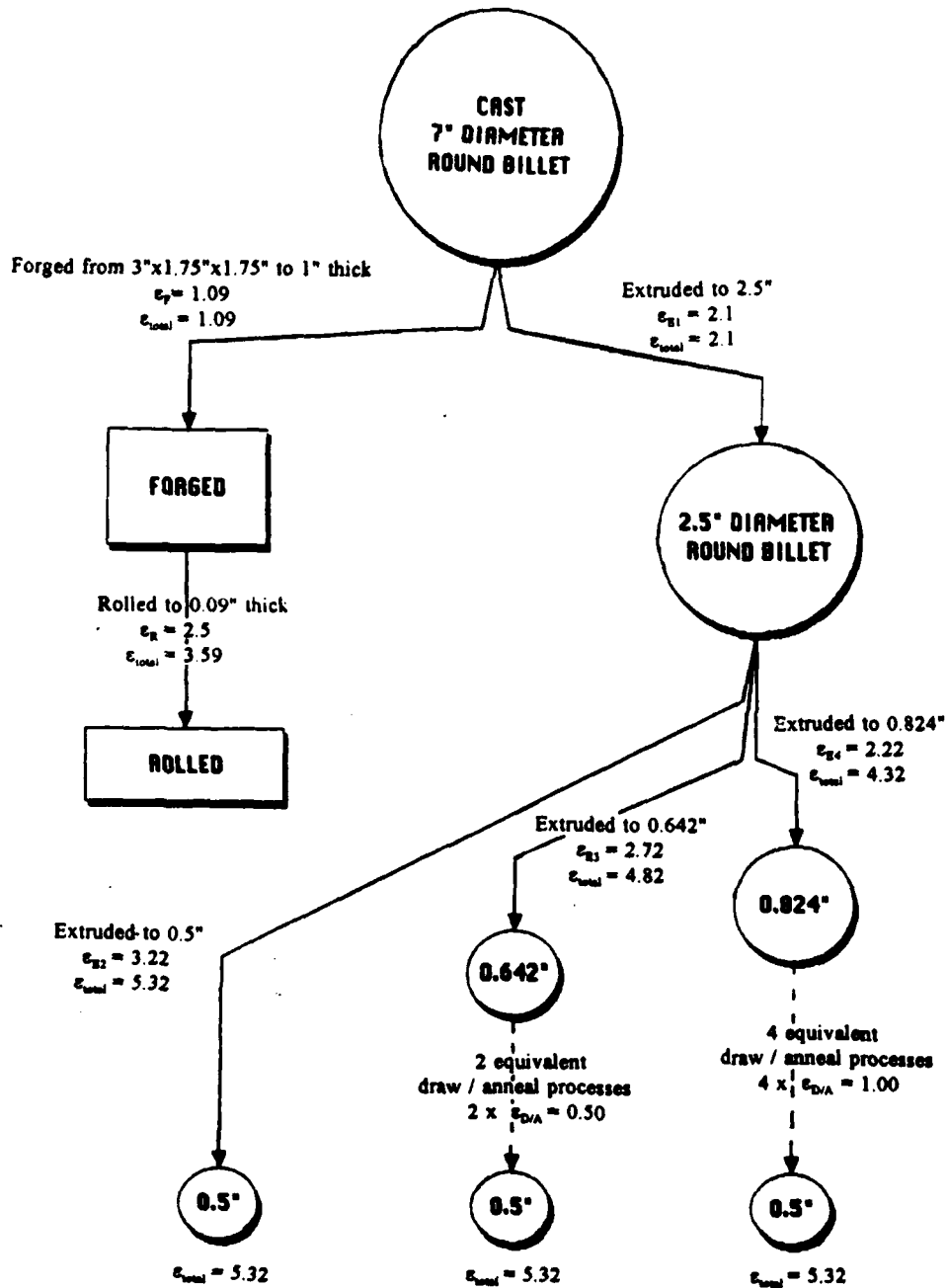


Figure 2: Processing Schedule for the Al 6061-Al₂O₃ Metal Matrix Composite. Size dimensions and strains are listed for each process.

of 0.25 each time to manufacture the 0.5 inch (12.7 mm) diameter bar. The intermediate anneals were all conducted at $T = 350^{\circ} \text{C}$ for 30 minutes.

B. DESIGN AND MACHINING OF TENSILE SPECIMEN

Previous work on MMCs at NPS involved tensile testing of sheet-type tensile coupons [Refs. 6, 7, 8, 14, and 15]. Material used in this thesis was provided as 0.5 inch (12.7 mm) round bar, requiring that a buttonhead type tensile specimen be designed.

Buttonhead grips were supplied by Applied Test Systems, Inc. of Saxonburg, PA. A tensile test specimen suitable for these grips was designed and is shown schematically in Figure 3. An additional design requirement was to keep the stress in the shoulder (intermediate diameter section) of the tensile specimen below the yield strength even when the corresponding stress level in the gage section attained the ultimate tensile strength. Care was taken to prevent stress in the shoulder from exceeding 90 MPa (a value below the elastic limit of solution-treated material) while still allowing the shoulder to slide through the buttonhead holder.

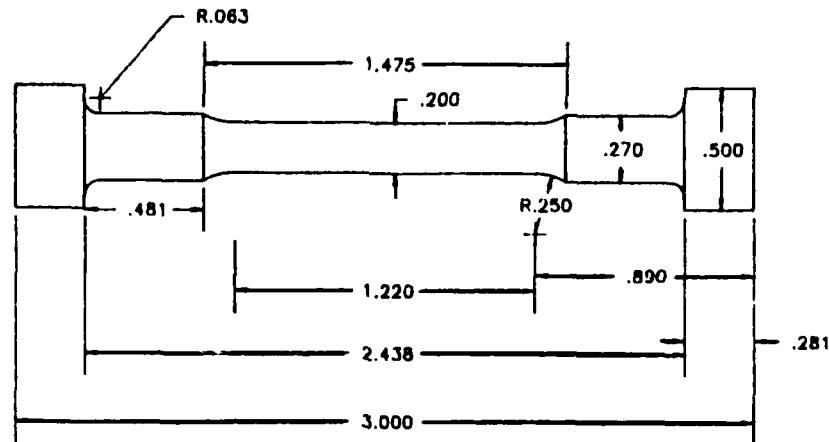


Figure 3: Tensile Test Buttonhead Design. These samples were machined from 0.5 inch (12.7mm) diameter extruded bars. (All numerical values provided in inches).

A check was also made to ensure that the grip ends of the buttonheads would not shear prior to the fracture inside the gage section. The gage section length was at least four times the gage diameter.

Initial planning involved a final extrusion diameter of 0.375 inch (9.5 mm). A buttonhead design for such a diameter required an insert to be designed to properly hold the tensile specimen. Designs of both the buttonhead and the insert for this smaller diameter bar are included as Figure 4 (a) and (b).

Machining of 6061 Al buttonhead tensile samples was accomplished using a Hardinge lathe. High-speed steel tool bits were used to produce the desired radii and coolant was employed to minimize heat buildup. Machining of the 10 v/o Al_2O_3 MMC will require the same lathe and the proper size polycrystalline diamond (PCD) tipped tool bits to allow production of the tensile specimen [Refs. 16 and 17].

Initial evaluation of this specimen design revealed a tendency of 6061 Al samples to fracture near one end of the gage section. This was determined to be the result of machining practice. These procedures were altered such that the initial plunge cut to create the 0.2 inch (5.1mm) diameter gage section was taken randomly along the region of the gage section. This resulted in samples which fractured near the center of the gage.

C. HEAT TREATING

In this work, a solutionizing temperature of 560°C was used for both the MMC and the unreinforced 6061 aluminum. This temperature was also used in earlier work, e.g. [Ref. 18]. The necessary duration for solution heat treatment (SHT) was determined to be 70 minutes [Ref. 19].

Heating was accomplished in a Lindberg type 51222 furnace. A K-type thermocouple, with the wire wrapped around the sample, was used to monitor the temperature. Samples were placed on an aluminum alloy structural channel which had been

E. MECHANICAL TESTING (HARDNESS AND TENSILE)

Hardness was measured using a Rockwell Hardness Tester (Model 1 JR), with a 1/16 inch diameter ball and a 60 kg load to measure the hardness on the "F" scale. The measured values were then corrected due to the workpieces being cylindrical [Ref. 20]. A comparison of the hardnesses of the unreinforced matrix and the MMC will be discussed in the results section.

Tensile buttonhead samples for each aging condition of the unreinforced 6061 Al were pulled using an Instron Model 4507 testing machine. Data was processed within the Instron Series IX Automated Materials Testing System. All tests were conducted at ambient temperature. A sample rate of 2 points per second and a crosshead speed of 1.0 mm/min, corresponding to a nominal strain rate of $5.4 \times 10^{-4} \text{ s}^{-1}$, was utilized during the tests. Load versus displacement and stress versus strain plots were produced by the Instron system which was interfaced with a Zenith PC and an HP Laser Jet printer. All testing was done without an extensometer due to the size of the gage section. Data reduction was accomplished in accordance with procedure explained in Metals Handbook [Ref. 20].

F. POLISHING SCHEDULE AND ANODIZATION

Standard polishing techniques as outlined in Metals Handbook [Ref. 21] and in previous NPS thesis work [Refs. 6, 7, 8, 14, and 15] were used as a guide. Specific procedures developed are shown in TABLE (1). Grinding of the cold mounted

allowed to equilibrate at the furnace temperature. This was done to ensure complete heating of the samples and record accurate temperature measurements. Additional thermocouples were placed on each side of the channel to monitor its temperature throughout the heating process.

In order to analyze the effect of the SHT temperature on the microstructure of the MMC matrix, two short sections of the twice extruded [0.5 inch (12.7 mm) diameter] MMC were sectioned. Only the 10 v/o material was studied and the MMC was solution treated for 70 minutes at each of the following temperatures: 480° C, 500° C, 530° C, and 560° C. These temperatures were chosen following a review of previous work by Eastwood which involved solutionizing at 500° C and 560° C [Ref. 6].

D. AGING STUDY

A study of aging response was done utilizing a Blue-M oven, Model OV-490A-3, at a temperature of 160°C. This temperature was selected again reflecting previous work by Eastwood [Ref. 6]. As with the SHT, the samples were placed on an aluminum alloy plate to ensure thorough and even heating. The following times were chosen for uniform coverage of a logarithmic time axis: 10 minutes, 24 minutes, 56 minutes, 133 minutes, 316 minutes, 750 minutes, 1778 minutes, 4217 minutes, and 10,000 minutes.

TABLE I: POLISHING SCHEDULE

Step #	Polishing Mechanism	Polishing Medium	Lubricant	Wheel (RPM)	Time (min)	Comments
1	Knuth-Rotor 3	320 Grit	water	300	1 to 2	FEPA-P (Sinuer's standard grit scale) light pressure
2	Knuth-Rotor 3	500 Grit	water	300	1 to 2	FEPA-P (Sinuer's standard grit scale) light pressure
3	Knuth-Rotor 3	1000 Grit	water	300	2 to 5	FEPA-P (Sinuer's standard grit scale) light pressure
4	Knuth-Rotor 3	2400 Grit	water	300	5 to 10	FEPA-P (Sinuer's standard grit scale) moderate pressure
5	Buehler Standard Polishing Table	6 micron DP-spray	DP red	400	5 to 10	Buehler's Solvyl Cloth moderate pressure
6	Buehler Standard Polishing Table	1 micron DP-spray	DP red/ metalcl	400	5	Buehler's Micro Cloth light pressure
7	Buehler Standard Polishing Table	0.25 micron DP-spray	DP red	400	3	Buehler's Micro Cloth light pressure
8	Buehler Low Speed Polishing Table	0.05 colloidal silica	DP red/ water	180-200	6	Buehler's Micro Cloth light pressure (wore gloves)

samples was accomplished using a Struers' Knuth-Rotor-3 while polishing utilized a standard Buehler polishing table. Polishing cloths used were Buehler microcloth and Buehler Selvyt cloth, each having a very light nap. Both Struer DP Red lubricant and Buehler Metadi Fluid extender were used at various stages. Most time was consumed during grinding on 2400 grit and 6 micron diamond spray polishing wheels. Only minimal particle pullout was observed for the MMC material.

In order to examine the matrix microstructure of the MMC, the samples were anodized in Barker's Reagent (5.5ml HBF_4 + 95ml H_2O + 0.7g Boric Acid). Metal studs were screwed through the cold mount to provide contact with the sample. A voltage of 10 VDC was applied for 60 seconds at ambient temperature to provide the desired grain contrast.

G. OPTICAL MICROSCOPY

Polished samples representing the various processing stages, from an as-cast to a twice-extruded 0.5 inch (12.7 mm) diameter bar, were examined using a Zeiss ICM-405 optical microscope. Polished samples were photographed with the same Zeiss optical microscope using Polaroid type 55 positive-negative film. The negatives were processed using a sodium sulfite solution, a water bath, and finally a Kodak Photo Flo 200 solution rinse. Anodized samples were examined using crossed polars and photographed using a Zeiss Universal Photomicroscope. Standard 35mm film (TMY 400) was utilized

for these photographs. A Bausch and Lomb stage micrometer (both metric and English units) was utilized to scale the photographs.

H. IMAGE ANALYSIS

Polaroid photographs were scanned into a (.tif) file using an image scanner and Adobe Photoshop 2.5 software. These files were analyzed using Image Pro Plus 2.0 software to determine the particle area, aspect ratio (major axis / minor axis), angle between a vertical axis and a major axis of the particle, the grid position (x, y) of the particle's centroid, the maximum diameter of the particle and the average diameter of the particle.

For each particle, the software determines the lengths of a chord from one surface to the opposite passing through the centroid. The initial chord is along the horizontal direction with each subsequent chord rotated clockwise in five degree increments. The maximum diameter is the maximum chord length determined, while the average particle diameter is the average of the 36 values measured for each particle. These data were then entered into a spread sheet file using Microsoft Excel 4.0 for Windows. Histograms of the aspect and maximum diameter data were then produced for the various processing conditions. The number of histogram bins, N , was generated utilizing the Sturgis Rule:

$$N=1+3.3\log(n)$$

(6)

where n is the number of particles counted. NNDs for each particle in the photomicrographs, of each processing condition, were computed using a Fortran code included as APPENDIX A.

IV. RESULTS

A. THE EFFECT OF PROCESSING STRAIN ON PARTICLE DISTRIBUTION

1. Visual Interpretation of The Microstructure

Photomicrographs of the as-polished MMC were obtained at various stages of the TMP. To obtain a more complete representation of the strain dependence of the particle distribution, samples from the concurrent work by Hoyt [Ref 13] on rolling of these materials were also examined. The flow paths were previously shown in Figure 2 for both processes. These photomicrographs are shown in Figures 5 through 11 and show several notable features.

First, the clustering of the reinforcement particles, seen primarily in the as-cast condition, Figure 5, tends to become less prominent in the initial stages of processing (i.e., forging or extrusion to 2.5 inches). Particle clustering occurs during solidification; the initial deformation processing deforms these clusters into bands (e.g. Fig. 6) and further straining appears to disperse these bands.

Banding persisted until a total processing strain of at least 4.0 was reached (Figs. 9, 10 and 11). The longest dimension of the reinforcement particles tended to become aligned in the working direction. Optical micrographs of

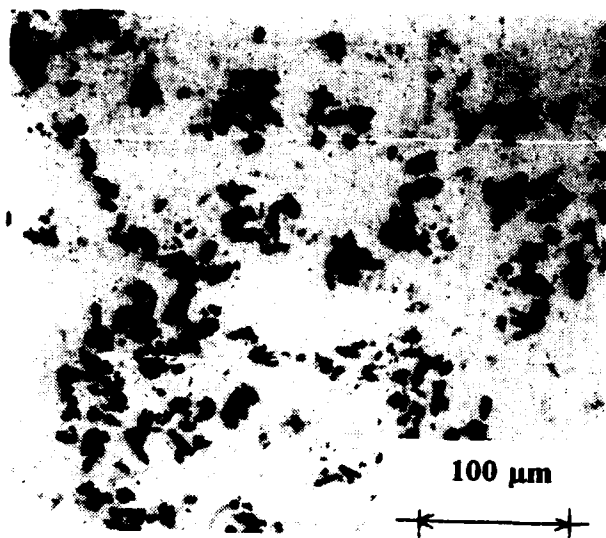


Figure 5:

Optical Micrograph of As-Cast Condition for Al 6061 - 10 v/o Al_2O_3 MMC. (200x) The S-plane is shown. Notice the clustering of reinforcement particles. (Photo provided by Ref. 13).

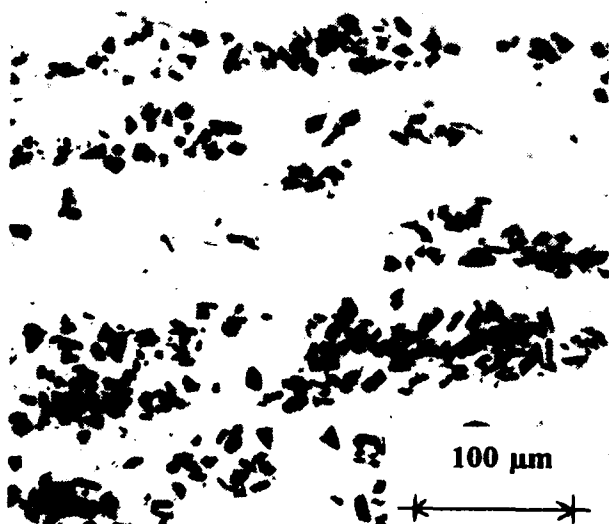


Figure 6:

Optical Micrograph of Forged Condition for Al 6061-10 v/o Al_2O_3 MMC. (200x) Notice the banding of particles in the working (horizontal) direction. (Photo provided by Ref. 13).

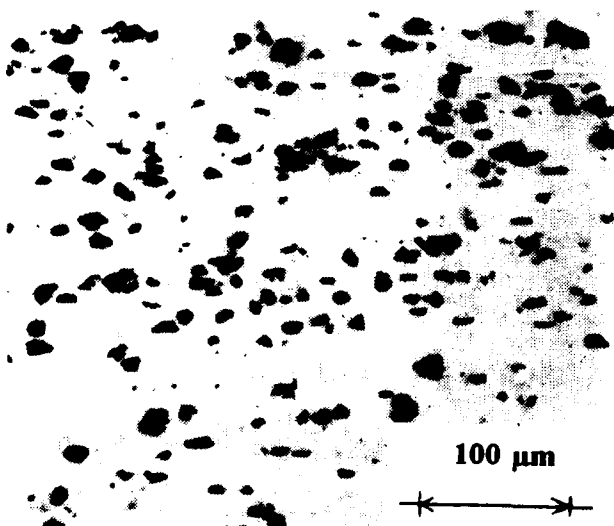


Figure 7:

Optical Micrograph of Rolled Condition for Al 6061-10 v/o Al_2O_3 MMC. (200x) Notice the continued existence of particle banding in the working (horizontal) direction. (Photo provided by Ref.13).

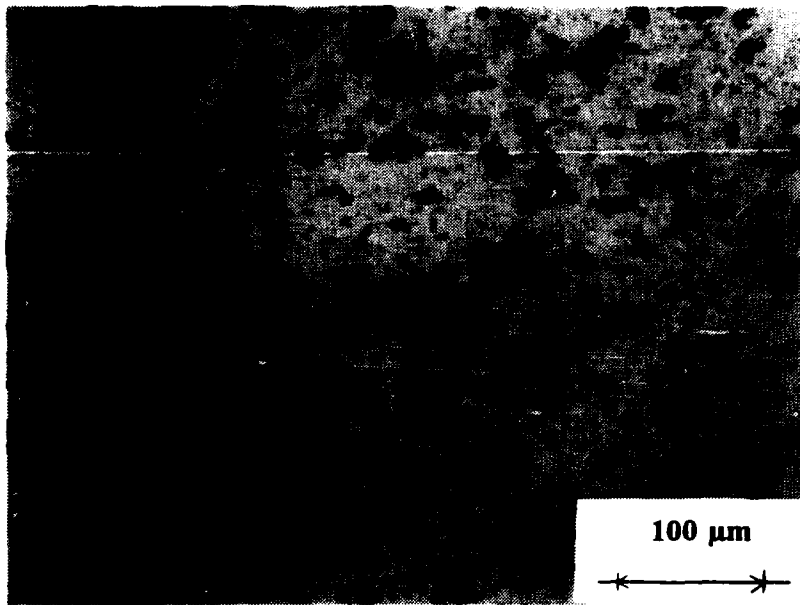


Figure 8: Optical Micrograph of Single Extrusion to 2.5 inches (63.5mm) Diameter Bar for Al 6061-10 v/o Al₂O₃ MMC. (200x) Processing strains shown in Figure 2. The longitudinal plane is shown. Notice the existence of banding in the working (horizontal) direction.

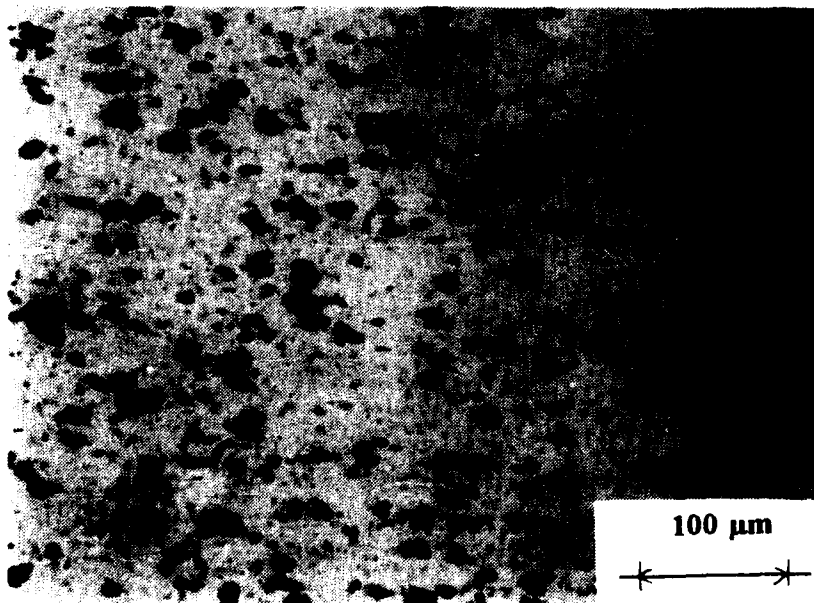


Figure 9: Optical Micrograph of Twice Extruded to 0.824 inches (20.9mm) Diameter Bar for Al 6061-10 v/o Al₂O₃ MMC. (200x) Processing strains shown in Figure 2. The longitudinal plane is shown. Notice the absence of banding.

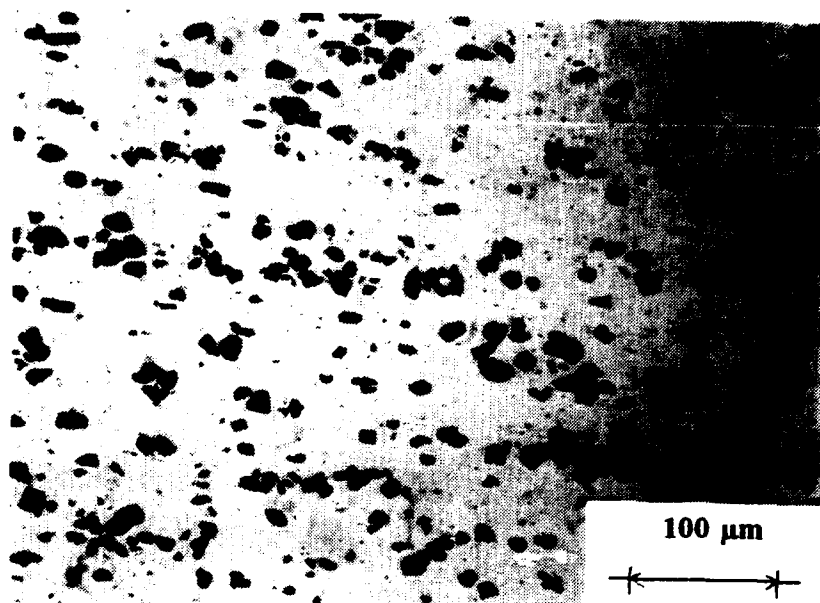


Figure 10: Optical Micrograph of Twice Extruded to 0.642 inches (16.3mm) Diameter Bar for Al 6061-10 v/o Al₂O₃ MMC. (200x) Processing strains shown in Figure 2. The longitudinal plane is shown. Notice the absence of banding.

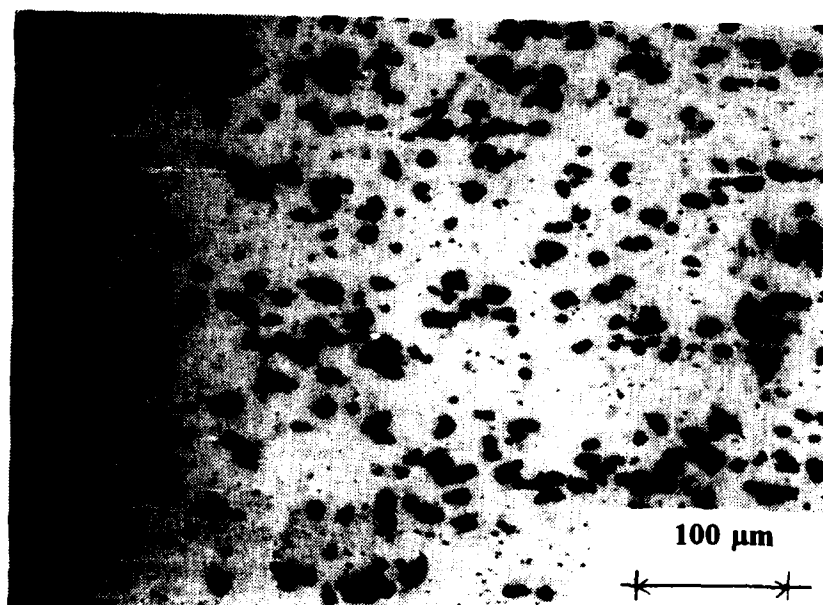


Figure 11: Optical Micrograph of Twice Extruded to 0.5 inches (12.7mm) Diameter Bar for Al 6061-10 v/o Al₂O₃ MMC. (200x) Processing strains shown in Figure 2. The longitudinal plane is shown. Notice the absence of banding.

transverse sections from the extruded product did not indicate any evidence of such banding for any amount of strain.

Samples of the once-extruded [2.5 inch (63.5 mm) diameter] and the twice-extruded [0.5 inch (12.7 mm) diameter] MMC were SHT'd at 560⁰ C. Examination of Figures 12 (a) and (b) and 13 (a) and (b) revealed no noticeable effect on the distribution of Al₂O₃ particles compared to the as-received or as-extruded condition. SHT does reduce the amount of the Mg₂Si (the finer, gray particles) phase.

2. Computational Analysis of Photomicrographs

The mechanical properties of MMCs have been linked to the uniformity of the distribution of reinforcement particles (Refs. 3, 6, 22, and 23). Here, an attempt was made to quantify the uniformity of the reinforcement particles by measurement utilizing image analysis. As-polished samples representing each stage of both the rolling and extrusion operations were examined. Several features were analysed as described earlier.

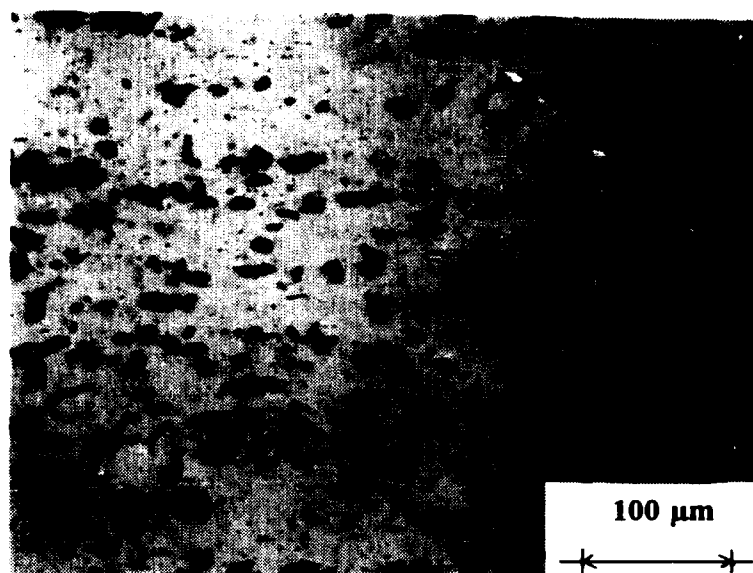


Figure 12(a): Optical Micrograph of Single Extrusion to 2.5 inches (63.5mm) Diameter Bar. (200x) The longitudinal plane is shown with the working direction in the horizontal plane. The sample is in the as received condition.

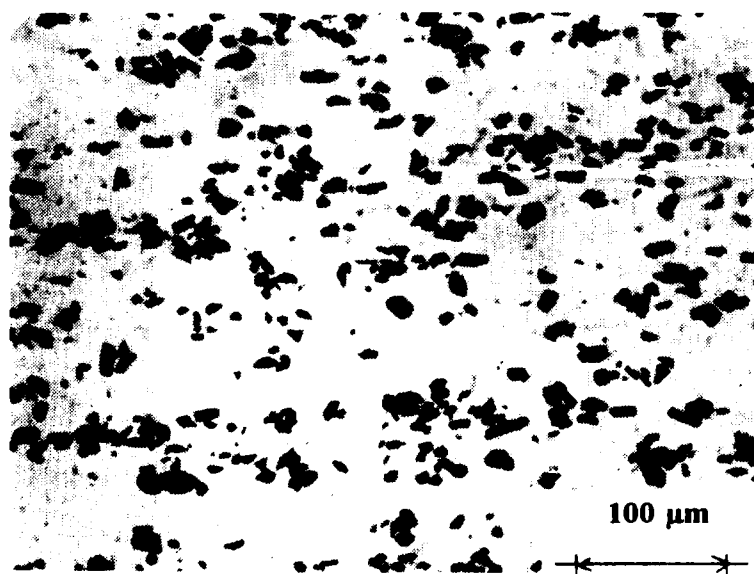


Figure 12(b): Optical Micrograph of Single Extrusion to 2.5 inches (63.5mm) Diameter Bar. (200x) The longitudinal plane is shown with the working direction in the horizontal plane. The sample has been solution heat-treated for 70 minutes at 560°C.

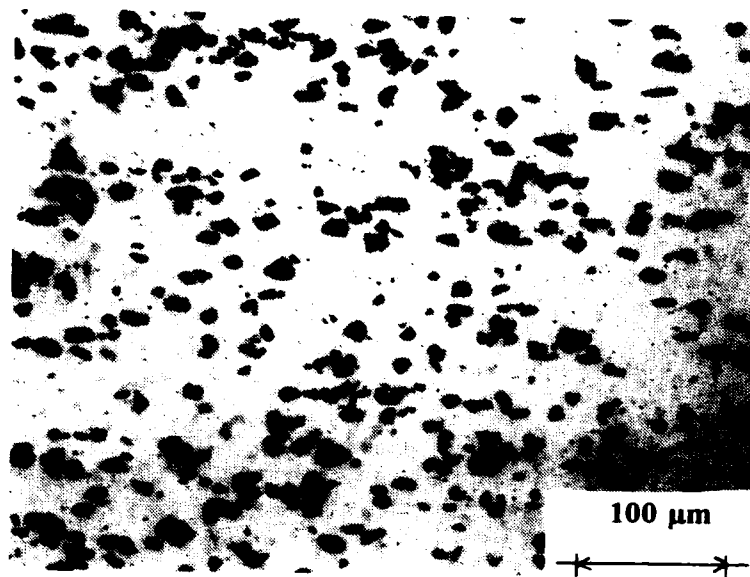


Figure 13(a): Optical Micrograph of Twice Extruded to 0.5 inches (12.7mm) Diameter Bar. (200x) The longitudinal plane is shown with the working direction in the horizontal plane. The sample is in the as received condition.

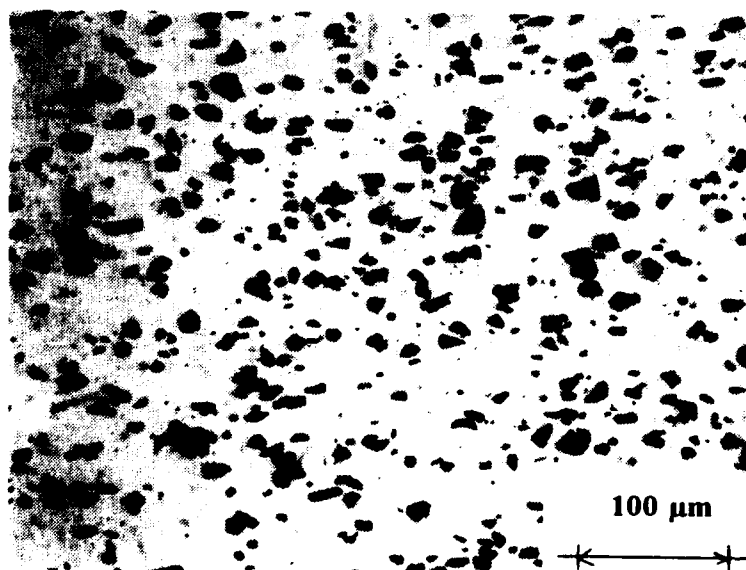


Figure 13(b): Optical Micrograph of Single Extruded to 0.5 inches (12.7mm) Diameter Bar. (200x) The longitudinal plane is shown with the working direction in the horizontal plane. The sample has been solution heat-treated for 70 minutes at 560° C.

Average values for the particle aspect ratio, maximum diameter, and mean diameter are listed in TABLE II. These values, plotted in Figures 14, 15, and 16, show no significant change in mean aspect ratio, mean maximum particle diameter, and mean particle diameter, as the value of the accumulated processing strain is increased. This indicates that the particles are not being fractured during these TMPs.

TABLE II: FIRST NEAREST NEIGHBOR DISTANCES ASPECT RATIOS, MAXIMUM PARTICLE DIAMETER, AND AVERAGE PARTICLE DIAMETER FOR VARIOUS PROCESSING CONDITIONS SHOWN IN FIGURE 1.

Process Condition	Total Strain	F & R NND	EXTR NND	F & R Aspect	EXTR Aspect	F & R Max Part D	EXTR Max Part D	F & R Avg Part D	EXTR Avg Part D
As Cast (7" diameter billet)	0	11.32	11.32	2.01	2.01	10.60	10.60	7.84	7.84
Forged to 1" thick	1.09	10.92		2.18		10.43		7.56	
Extruded to 2.5" diameter (as rcvd)	2.1		12.07		2.07		10.78		7.86
Extruded to 2.5" diameter (ST'd)	2.1		11.41		1.95		10.66		7.96
Rolled to 0.09" thick	3.59	13.28		2.15		10.46		7.58	
Extruded further to 0.824" from 2.5"	4.32		11.99		1.99		9.94		7.44
Extruded further to 0.642" from 2.5"	4.82		12.9		1.81		10.96		8.34
Extruded further to 0.5" from 2.5" (as rcvd)	5.32		12.58		1.94		10.82		8
Extruded further to 0.5" from 2.5" (ST'd)	5.32		11.72		2.12		9.7		7.14

Key: St'd Solution heat treated at 560° C for 70 minutes
F & R Forged and rolled processing path
Extr Extruded processing path
NND First nearest neighbor distance (microns)
Aspect Aspect ratio (max diameter/min diameter)
Max Part D Maximum particle diameter
Avg Part D Mean particle diameter

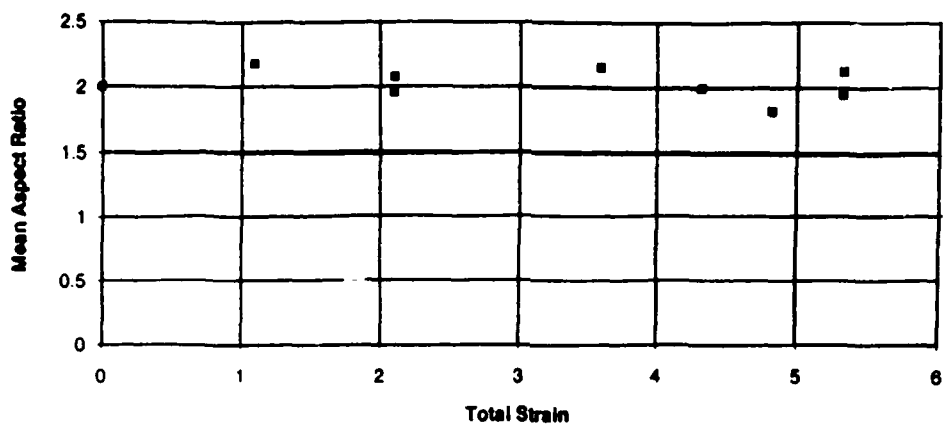


Figure 14: Plot of Mean Aspect Ratio vs. Total Processing Strain.

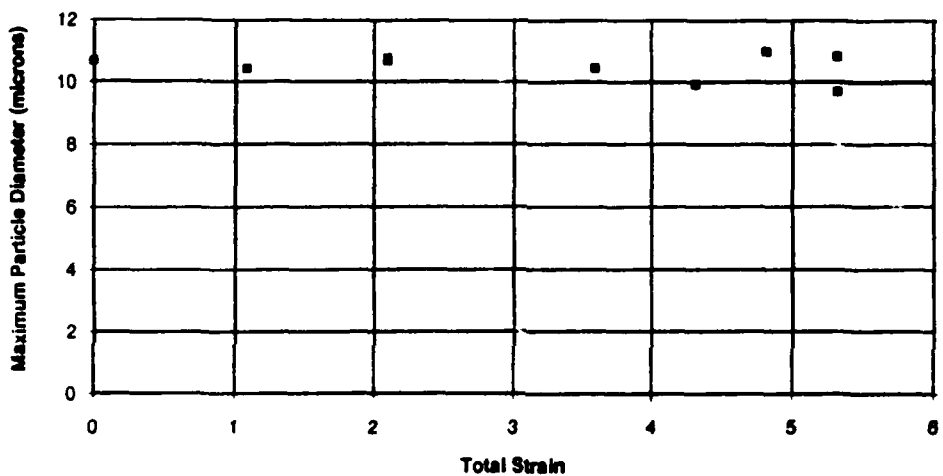


Figure 15: Plot of Maximum Particle Diameter vs. Total Processing Strain.

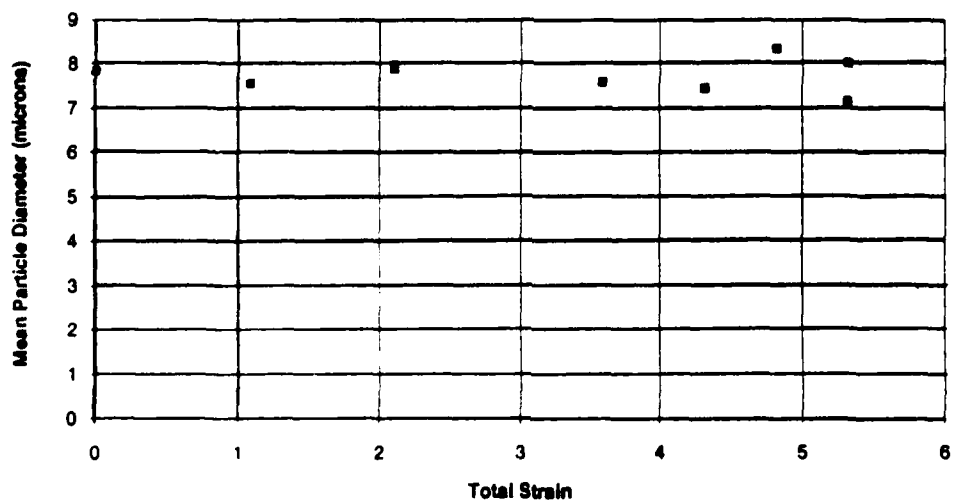


Figure 16: Plot of Mean Particle Diameter vs. Total Processing Strain.

The mean NND values, (which were calculated using the particle centroid locations), were included as TABLE II and are repeated in TABLE III along with additional values for the NND predicted by equations 2 and 3. Using the number of particles analyzed by the software and the area of the grid which had been analyzed, the values of N_A (number of particles per unit area) and apparent area fraction of particles were calculated. These are also included in TABLE III. There appears to be a slight trend towards increased NND values with increased process strain in the interval of strain from 1.0 to 3.0, (Figure 17). In this regime, particle redistribution is occurring and clusters are being dispersed. The increase in measure NND may reflect these processes and a similar slight change had been noted in the simulations [Ref. 9]. Beyond a strain of 3.0 the NND appears to become constant. The small changes in NND would require further assessment prior to use as a quantitative tool for describing the homogeneity of the particle distribution. The apparent area fraction does not appear to vary systematically. Values obtained are generally greater than the nominal particle volume fraction (0.1). Metallographic preparation and determination of the particle extent during image analysis both may affect this parameter. The variation from one sample to the next may also reflect long-range variation in particle volume fraction in the composite.

TABLE III: MEAN NEAREST NEIGHBOR DISTANCES (CALCULATED AND OBSERVED)

Process Condition	Total Strain	Number of Particles	Particles per square micron	Area Fraction	Poisson Distribution mean NND	Image Analysis mean NND	Hexagonal Array mean NND
As Cast (7" diameter billet)	0	639	0.001411	0.091	13.31	11.32	28.62
Forged to 1" thick	1.09	844	0.001861	0.11	11.59	10.92	24.92
Extruded to 2.5" diameter (as rcvd)	2.1	804	0.001778	0.103	11.86	13.28	25.51
Extruded to 2.5" diameter (ST'd)	2.1	905	0.00201	0.129	11.15	12.07	23.98
Rolled to 0.09" thick	3.59	908	0.00366	0.138	8.26	11.41	17.76
Extruded further to 0.824" from 2.5"	4.32	987	0.00222	0.139	10.61	11.99	22.82
Extruded further to 0.642" from 2.5"	4.82	810	0.001781	0.138	11.85	12.9	25.47
Extruded further to 0.5" from 2.5" (as rcvd)	5.32	863	0.001889	0.123	11.51	12.58	24.74
Extruded further to 0.5" from 2.5" (ST'd)	5.32	1021	0.00219	0.114	10.67	11.72	22.95

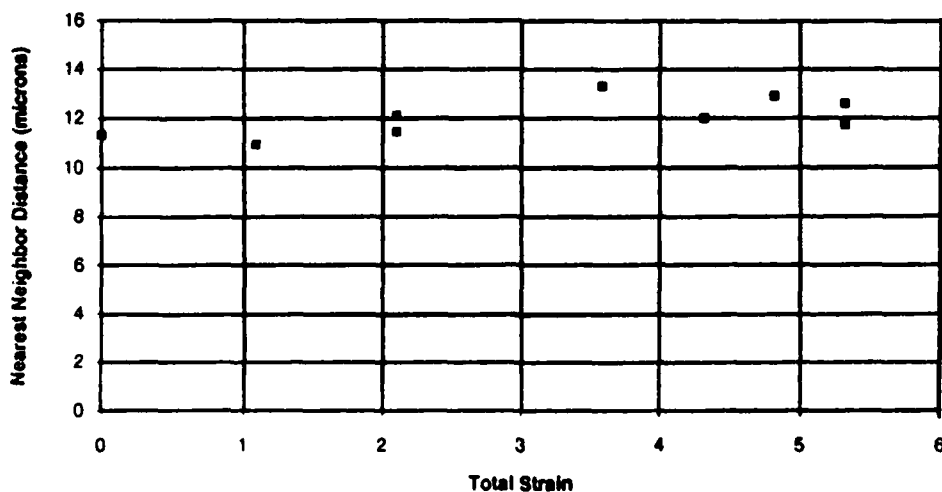


Figure 17: Plot of First Nearest Neighbor Distances vs. Total Processing Strain.

Computer simulations by Manfredi [Ref. 9] predicted that the NND for lognormally size distributed particles having an area fraction of 0.1 would be much nearer to the value for a Poisson distribution of points than to the NND of a uniformly spaced hexagonal array (see Figures 1 (a) and 1 (b)). This was also seen in the computer aided image analysis. Figure 18 shows a histogram for a twice extruded (0.50 inch (12.7 mm) diameter) MMC in the as received condition. The values of δ_{Hex} , δ_{Theo} , and δ_{Obs} are also indicated. Additional data for NND and aspect ratio values are included in Appendix B.

Comparison of Figures 1 and 18 reveals a striking similarity between the MMC microstructures and the computer generated particle distributions. The NND distributions are also similar (absolute scales are different), suggesting that the microstructure in Figure 18 is a random particle distribution in which has been achieved at this point in the processing. These observations also suggest that there is no interaction of particles due to strain hardening in the matrix during plastic deformation.

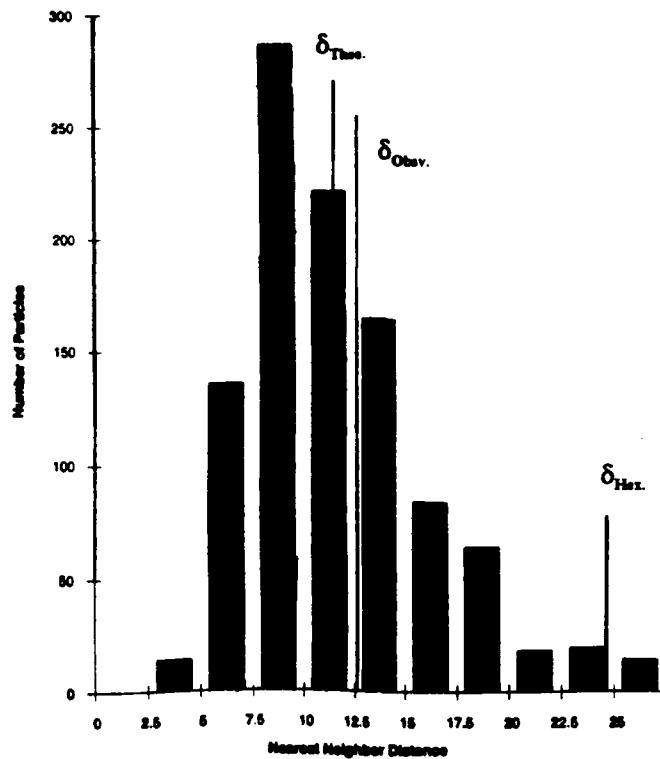


Figure 18(a): Histogram of First Nearest Neighbor Distances for Micrograph shown in Figure 18(b). "Delta" distance values (measured and calculated) are shown. Notice the resemblance to the curve for lognormal size distribution Figure 1(b).

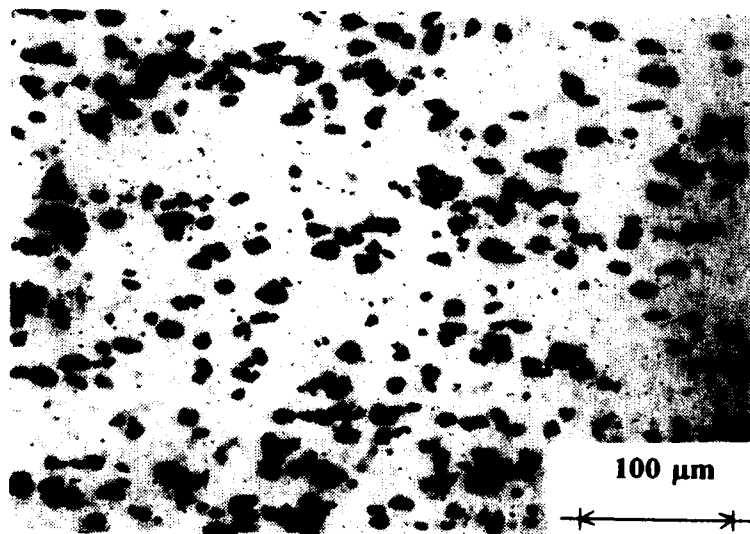


Figure 18(b): Optical Micrograph Repeated From Figure 13.

B. THE EFFECT OF PROCESSING STRAIN ON MATRIX GRAIN STRUCTURE

The samples previously examined in the as-polished condition were then anodized as described in the procedure section in order to investigate evolution matrix grain structure during this TMP. The effect of process strain was considered initially and samples of as-cast, once-extruded, and twice-extruded (Figure 2) materials were studied. The stability of grain structure during subsequent solution treatment was also assessed. During examination, polars were adjusted to allow the location of the particles within the matrix metal to be identified while maintaining sufficient orientation contrast to observe the grain structure.

1. Influence of Processing Strain

The as-cast microstructure, shown in Figure 19, consists of coarse grained matrix in addition to particle clusters. At this point, the grain size is about 125 microns. A non-uniform distribution of a second phase, likely Mg_2Si , reflects non-equilibrium solidification. Following homogenization and extrusion from 7.0 inches (177.8 mm) to 2.5 inches (63.5 mm) diameter (Figure 20), with a corresponding strain of $\epsilon_{Total} = 2.1$, a partially recrystallized matrix grain structure is apparent. Fine grains are seen within bands of reinforcement particles while coarser grains in between such bands are also evident. Some of the Mg_2Si also remains. This

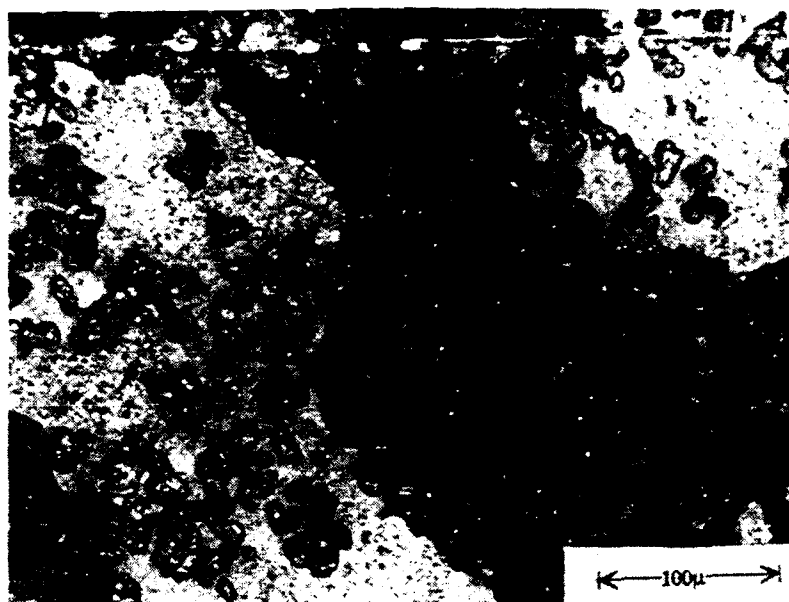


Figure 19: Anodized Photomicrograph of As-Cast Condition for a 6061-Al 10 v/o Al_2O_3 MMC. (250x) The longitudinal plane is shown.

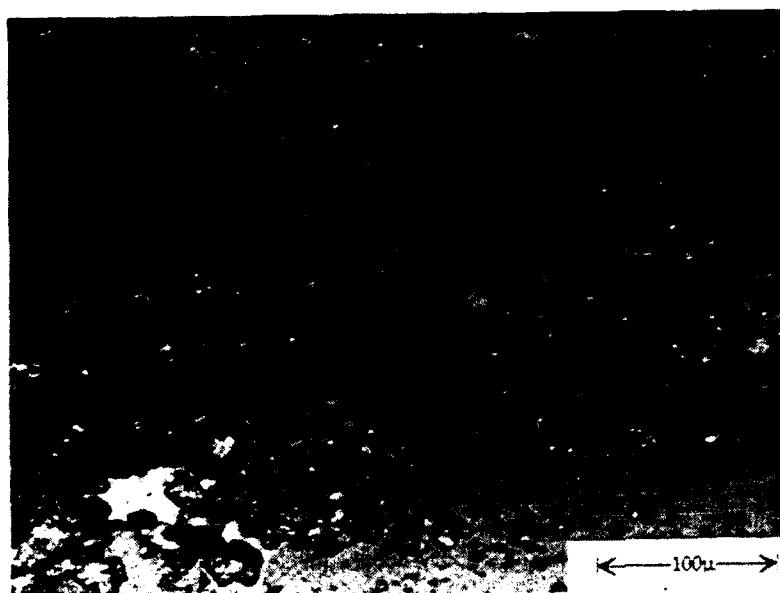


Figure 20: Anodized Photomicrograph of a Single Extruded to 2.5 inches (63.5mm) Diameter Bar. (250x) The longitudinal plane is shown).

phase is present as the finer, dark appearing particles in the microstructure.

The further straining due to the second stage extrusion produces a dramatic reduction in grain size as well as homogenization of the microstructure. This may be seen in Figure 21 a, b, and c. With redistribution of the particles, the matrix grain structure has become substantially more uniform. Furthermore, as the strain in the second extrusion stage becomes larger, the matrix grain size becomes finer. Mean linear intercept measurements of the grain size [Ref. 20], are summarized in TABLE IV and plotted in Figure 22. It is apparent that the grain size continues to be refined in association with homogenization of the particle distribution.

Particles often appear to be located on grain boundaries although many are within grains as well. The grain size based on PSN theory (equation 4) is estimated to be 28 microns, a value somewhat finer than the observed value of 37 microns. On the other hand, the Zener model (equation 5) predicts a grain size of approximately 80 microns. It is concluded that the PSN model, with some subsequent growth, best describes these results. A similar conclusion was reached by Humphreys, et al. [Ref. 24] in their study of Al-SiC composites containing similar particle volume fractions.

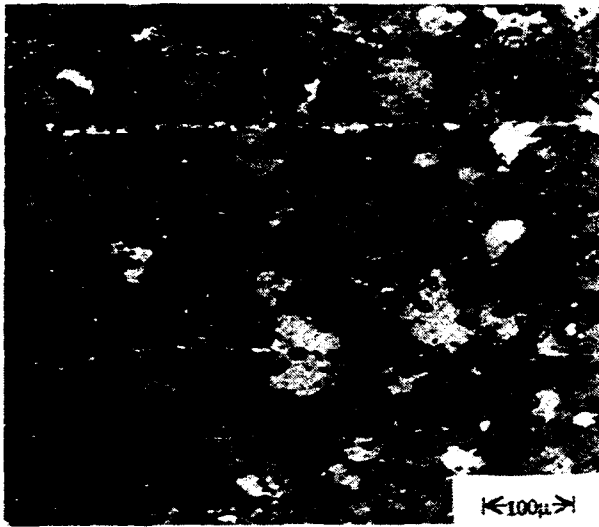


Figure 21 (a):

**Anodized Photomicrograph of a
Twice Extruded to 0.824 inches
(20.9mm) Diameter Bar. (125x)
The longitudinal plane is shown.**



Figure 21 (b):

**Anodized Photomicrograph of a
Twice Extruded to 0.642 inches
(16.3mm) Diameter Bar. (125x)
The longitudinal plane is shown.**

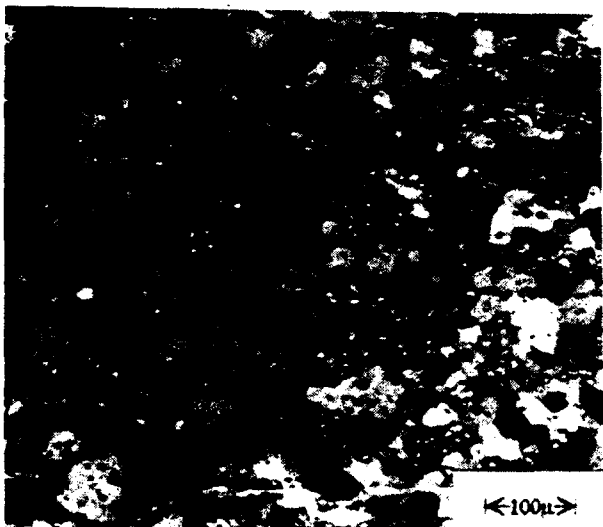


Figure 21 (c):

**Anodized Photomicrograph of a
Twice Extruded to 0.5 inches
(12.7mm) Diameter Bar. (125x)
The longitudinal plane is shown.**

TABLE IV: MATRIX GRAIN SIZES FOR VARIOUS TOTAL PROCESSING STRAINS

Process Condition	Average Matrix Grain Size (microns)
As Cast	123.8
1x Extruded to 2.5"	63.9
No SolutionHeat Treatment	
1x Extruded to 2.5"	56.1
70 min @ 560 C	
2x Extruded to 0.824"	44.1
No SolutionHeat Treatment	
2x Extruded to 0.642"	38.4
No SolutionHeat Treatment	
2x Extruded to 0.5"	36.8
No SolutionHeat Treatment	

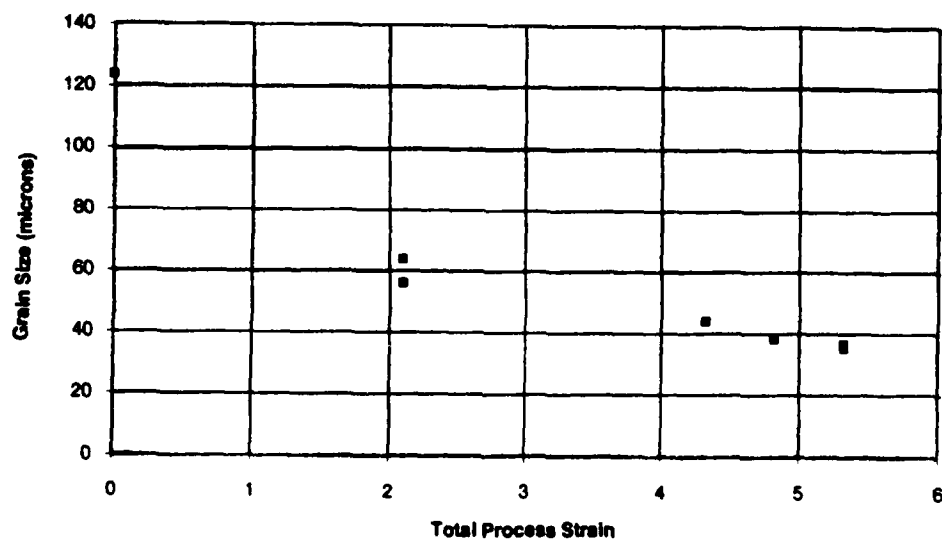


Figure 22: Plot of Matrix Grain Size vs. Total Processing Strain. Notice the decrease in matrix grain size with increasing processing strain.

2. The Effect of Solution Treatment

The final stage in the microstructure analysis considered the effect of subsequent SHT on microstructure. The results are shown in Figure 23 a thru e. Comparison of these microstructures (at a magnification of approximately 250X) reveals no difference in grain size for SHT temperatures varying from 480° C upward to 560° C. The solvus temperature appears to lie between 480° C and 500° C as the Mg_2Si remaining after extrusion disappears upon heating to 500° C. Nonetheless, no grain growth is seen, suggesting that the Mg_2Si provides no pinning effect to retard grain growth. Grain size measurements are presented in TABLE V where it is seen that the grain size is unaffected by SHT, remaining at about 37 microns.

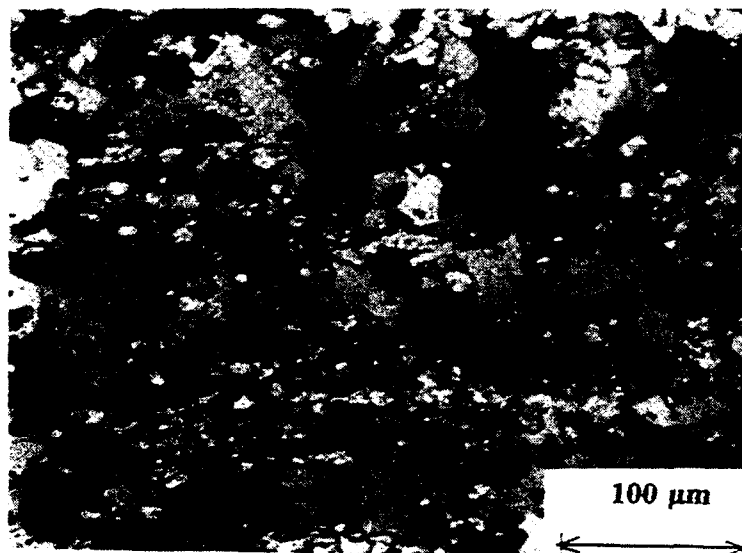


Figure 23 (a): Anodized Photomicrograph of a Twice Extruded to 0.5 inches (12.7mm) Diameter Bar. (250x) The sample is in the as-received condition.

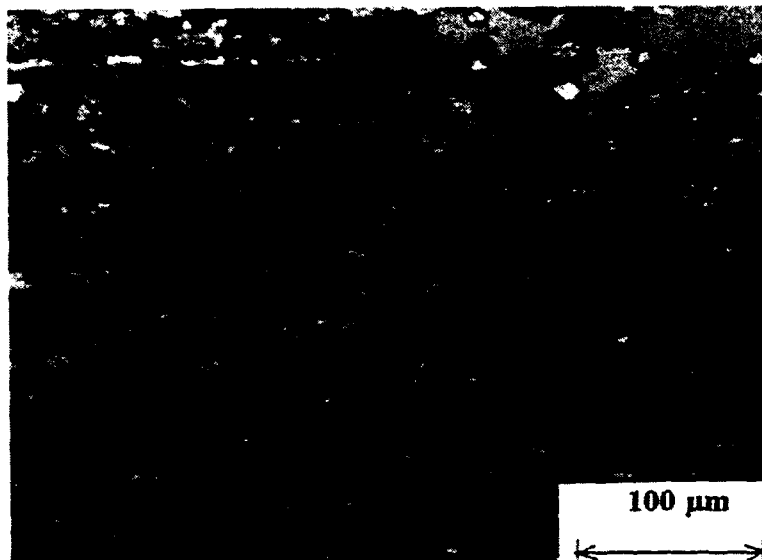


Figure 23

(b): Anodized Photomicrograph of a Twice Extruded to 0.5 inches (12.7mm) Diameter Bar. (250x) The sample has been solution heat-treated at 480° C for 70 minutes.

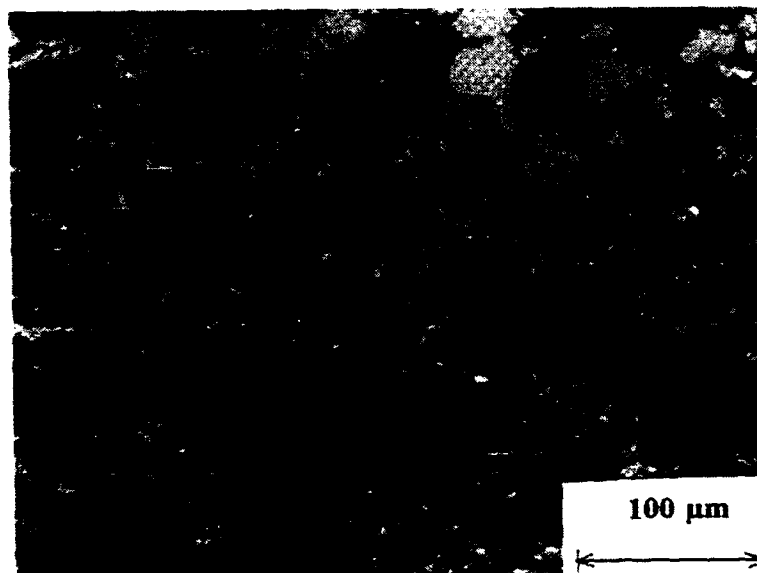


Figure 23

(c): Anodized Photomicrograph of a Twice Extruded to 0.5 inches (12.7mm) Diameter Bar. (250x) The sample has been solution heat-treated at 500° C for 70 minutes.

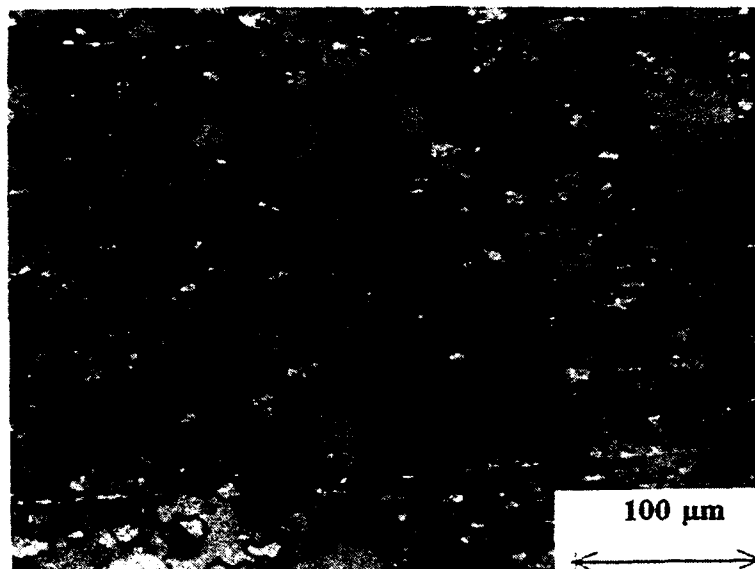


Figure 23 (d): Anodized Photomicrograph of a Twice Extruded to 0.5 inches (12.7mm) Diameter Bar. (250x) The sample has been solution heat-treated at 530° C for 70 minutes.

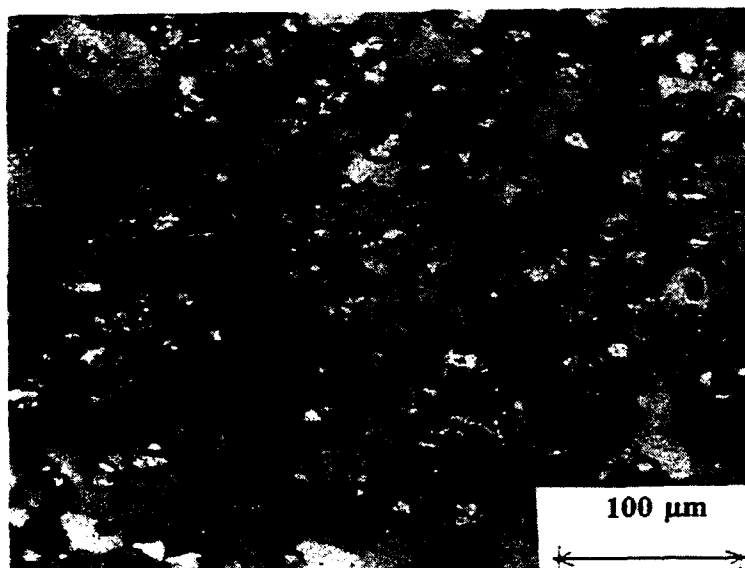


Figure 23 (e): Anodized Photomicrograph of a Twice Extruded to 0.5 inches (12.7mm) Diameter Bar. (250x) The sample has been solution heat-treated at 560° C for 70 minutes.

**TABLE V: THE EFFECT OF SOLUTIONIZATION TEMPERATURE
ON MATRIX GRAIN SIZE**

Process Condition	Average Matrix Grain Size (microns)
2x Extruded to 0.5" 70 min @ 480 C	37.1
2x Extruded to 0.5" 70 min @ 500 C	35.4
2x Extruded to 0.5" 70 min @ 530 C	37
2x Extruded to 0.5" 70 min @ 560 C	36.8

C. HARDNESS MEASUREMENTS OF UNREINFORCED 6061 AL AND A 10 V/O MMC

After solutionizing the unreinforced 6061 Al and the 10 v/o Al_2O_3 MMC (both of which were in the form of an extruded bar), a study of aging response was done and Rockwell F hardness values were measured. The hardness values, which required correction due to their measurement on cylindrical surfaces, were compared with hardness data obtained by Hoyt on rolled 10 v/o Al_2O_3 samples Ref [13]. These data are plotted in Figure 24. Hoyt's rolled 6061 Al- Al_2O_3 material had experienced either a 30 minute-interpass anneal or a 5 minute-interpass anneal. The data indicated that the extruded composite had a higher hardness and also reached peak hardness in less time, as compared to the unreinforced aluminum. Peak hardness values were similar for the extruded MMC, rolled MMCs, and unreinforced materials.

Finally, the hardness values for unreinforced 6061 Al (extruded bar vs. rolled flat) were compared to assess the tensile sample design discussed in Chapter III. These data are plotted in Figure 25. Data for the unreinforced rolled 6061 Al samples were provided by Hoyt [Ref. 13]. Hardness curves are nearly equivalent for the two differently processed unreinforced 6061 Al.

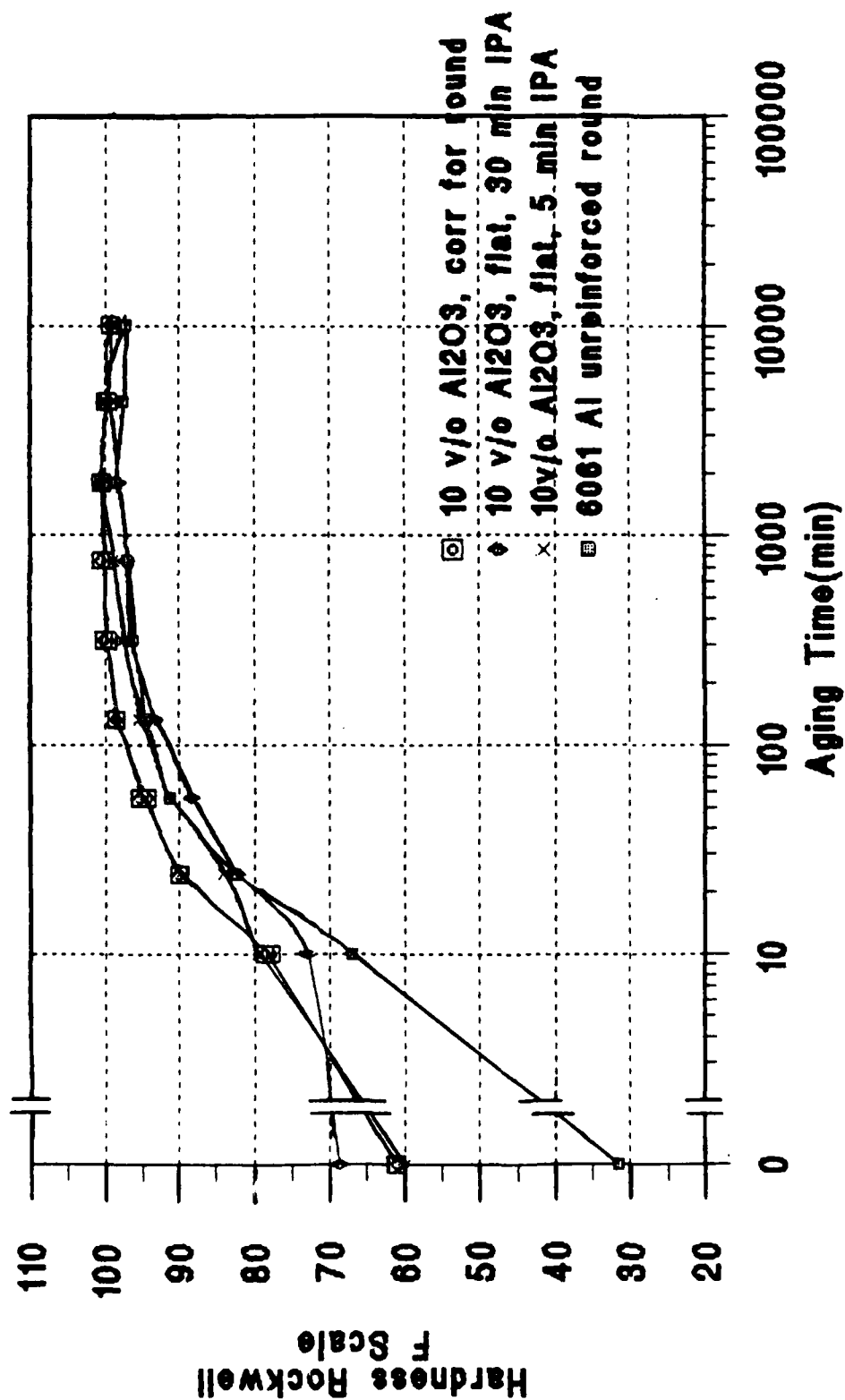


Figure 24: Hardness vs. Aging Time.
All samples were solution treated the appropriate amount of time at 560° C. Comparison of MMC to unreinforced 6061 Al.

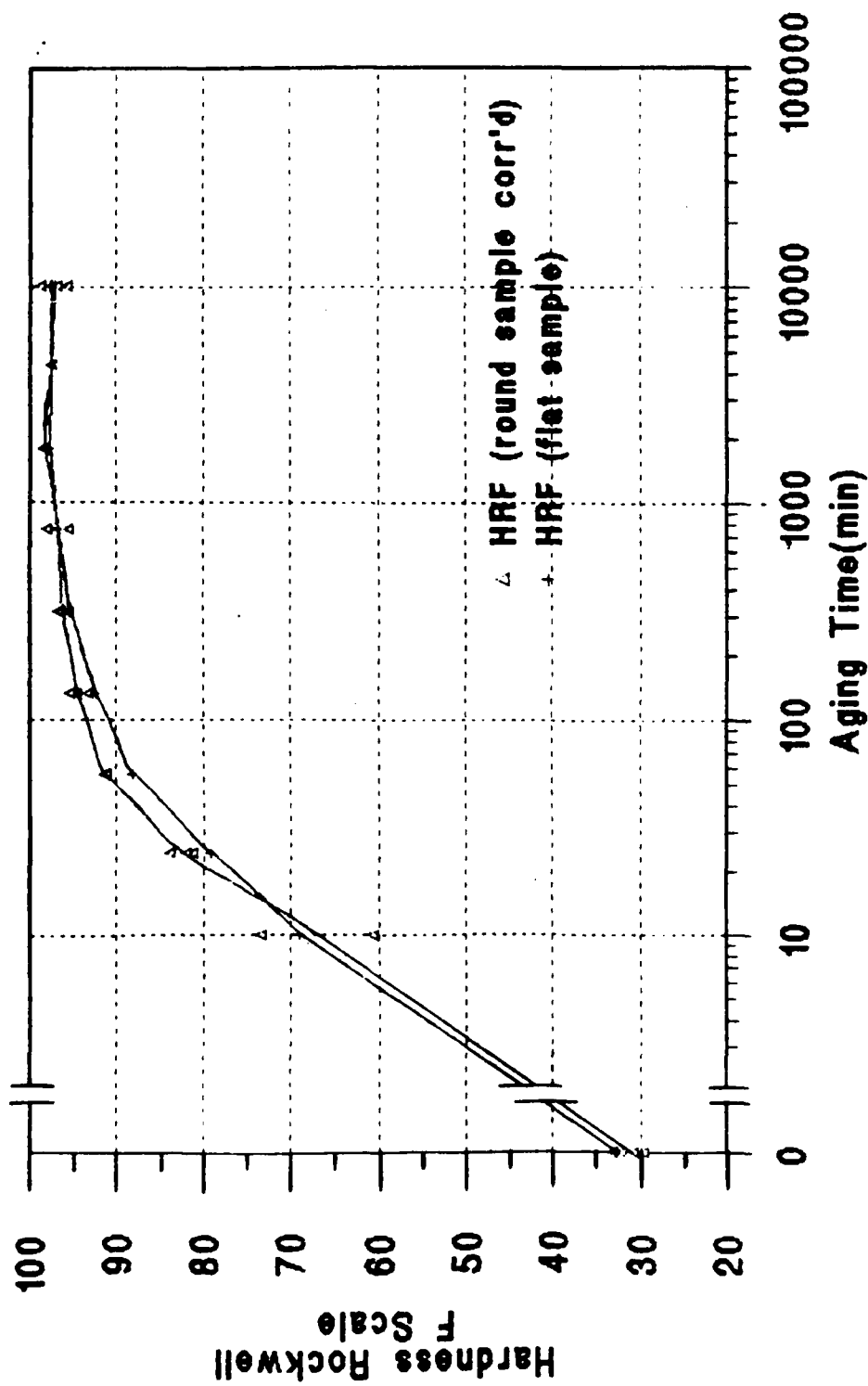


Figure 25: Hardness vs. Aging Time.
All samples were solution treated the appropriate amount of time at 560° C. Comparison of extruded round 6061 Al with rolled flat 6061 Al.

D. TENSILE TESTING OF EXTRUDED UNREINFORCED 6061 ALUMINUM

Mechanical testing of the unreinforced 6061 Al alloy was accomplished to assess the buttonhead sample geometry shown in Chapter III and to provide for future reference. Mechanical properties (i.e., ultimate tensile strength and 0.2% yield strength) of both the extruded buttonhead tensile test design and the flat tensile coupons design were compared after being solution treated and aged. Figures 26 and 27 are representations of these comparisons. Data for the unreinforced rolled 6061 Al samples were provided by Hoyt [Ref. 13]. The consistency of these mechanical property data with each other, as well as existing data for 6061 Al, indicate that the sample design is deemed satisfactory and should be used in future research.

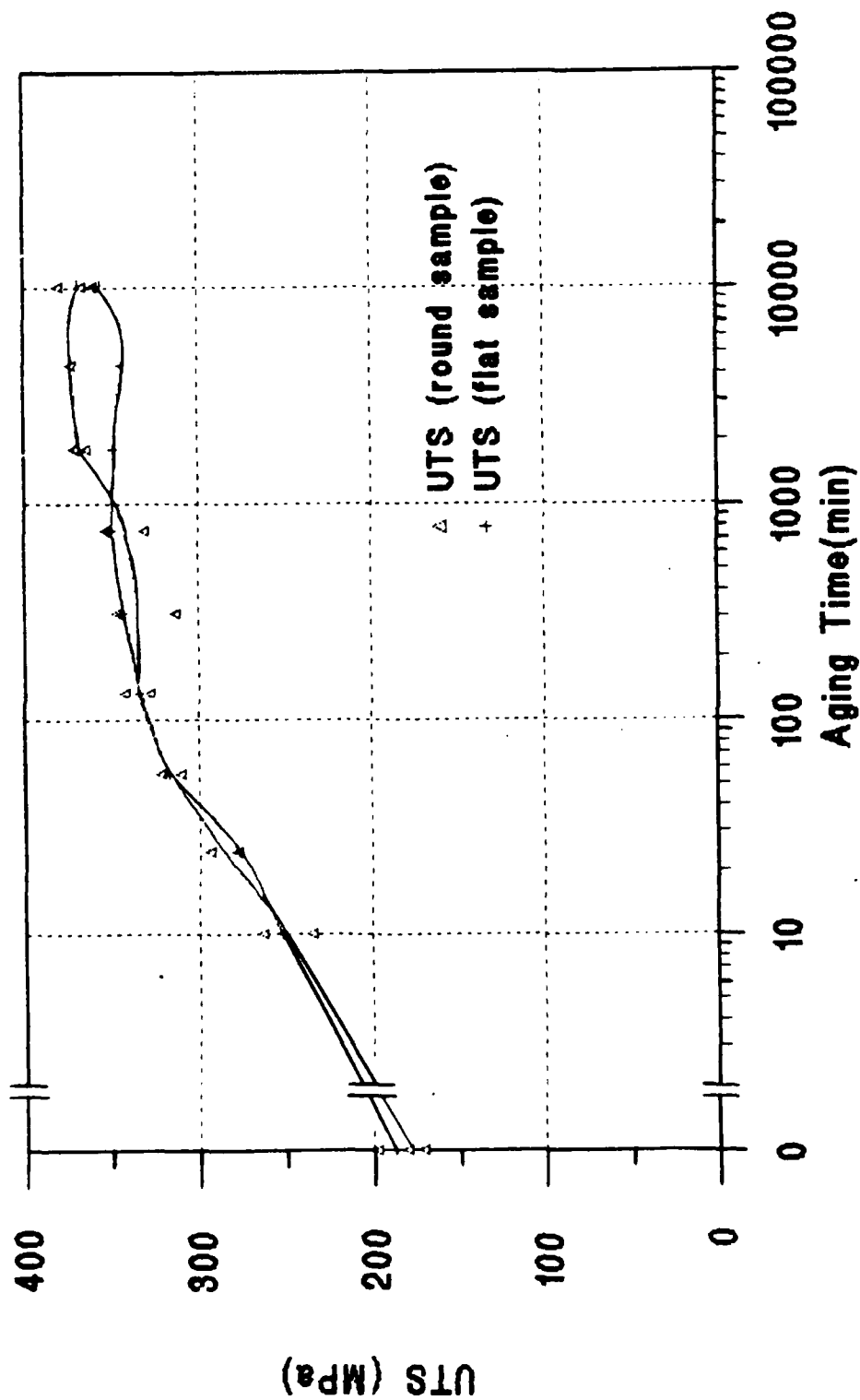


Figure 26: Ultimate Tensile Strength vs. Aging Time.
All samples were solution treated the appropriate amount of time at 560° C. Comparison of extruded round 6061 Al with rolled flat 6061 Al.

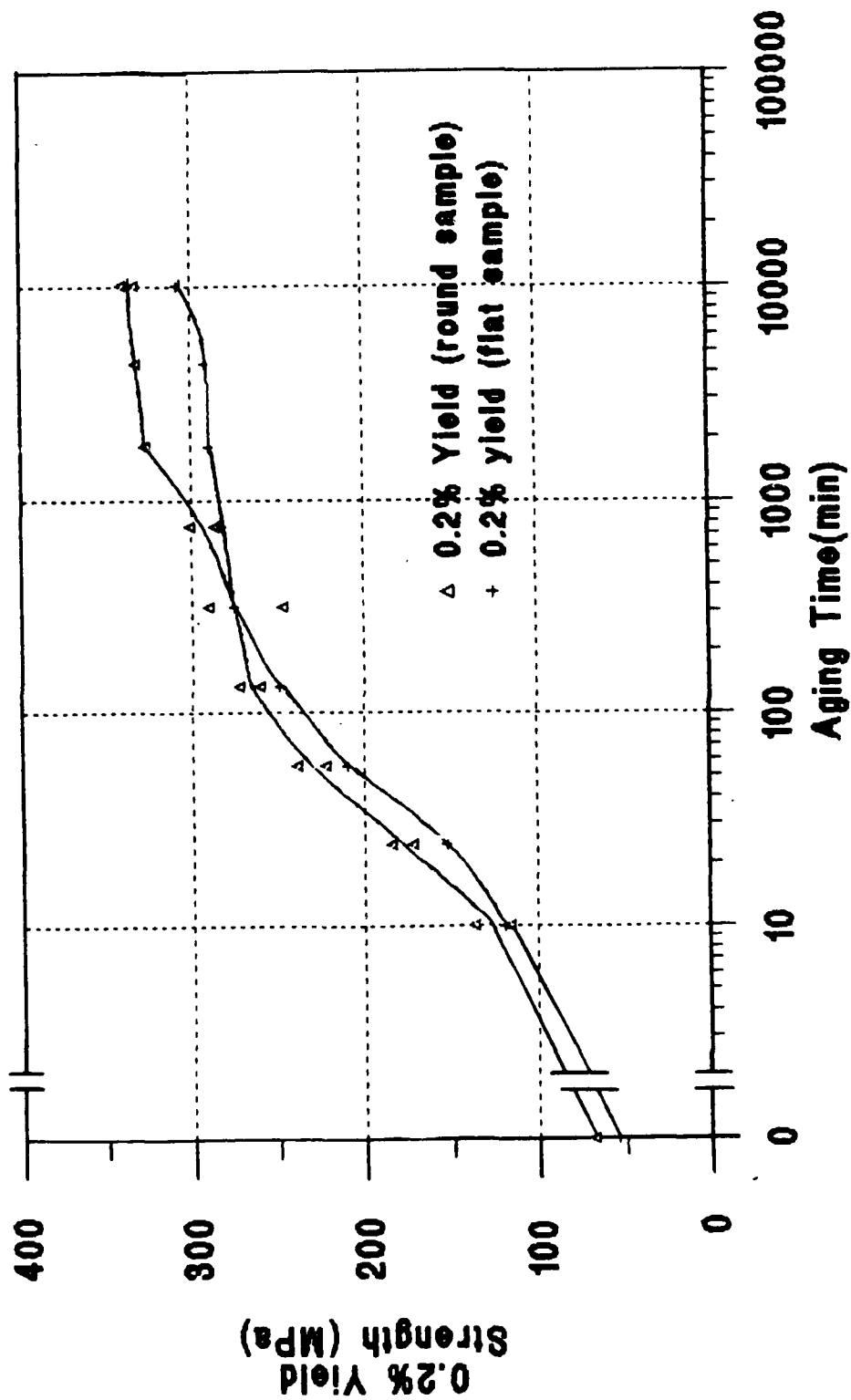


Figure 27: 0.2% Yield Strength vs. Aging Time.
 All samples were solution treated the appropriate amount of time at 560° C. Comparison of extruded round 6061 Al with rolled flat 6061 Al.

V. CONCLUSIONS

1. Particle clusters are dispersed by straining during processing.
2. Elimination of banding in the extrusions (due to the clusters for the as-cast condition) require strains on the order of 4.0.
3. Particles are not damaged during processing.
4. Computer simulations of random particle distributions provide accurate models of the actual particle distribution in fully homogeneous MMC material.
5. There does not appear to be a readily measured microstructural feature which provides a measure of homogenization during processing.
6. Refinement of the matrix grain structure takes place by PSN of recrystallization. As particles are redistributed during processing, grain size is reduced to a value of approximately 36 microns.
7. The grain size of fully processed material appears to be stable upon SHT at temperatures up to 560° C.
8. The MMC reaches peak hardness more rapidly than the unreinforced matrix alloy.
9. The tensile test sample geometry is satisfactory for further work.

VI. RECOMMENDATIONS FOR FURTHER STUDY

1. Investigate the effect of the draw/anneal cycles on the particle distribution and matrix grain size.
2. Examine microstructures of 1) above for evidence of particle damage during processing.
3. Investigate mechanical characteristics of the MMC (tensile testing and hardness testing) for all three processing routes (direct extrusion to 0.5 inch (12.7mm), two draw/anneals, and four draw/anneals) for both 10 v/o and 20 v/o.
4. Study the effects of various aging time and temperatures on the resulting mechanical characteristics of the extruded composite materials.

APPENDIX A

COMPUTER CODE (FORTRAN) FOR GENERATING FIRST NEAREST NEIGHBOR DISTANCES

```

C      program thsis1
C
C      THIS PROGRAM WILL CALCULATE THE NEAREST NEIGHBOR DISTANCE FOR
C      EACH OF A NUMBER OF REINFORCEMENT PARTICLE POSITIONS FOR AN
C      ARRAY OF IMAGE ANALYZED PARTICLES.
C
C      USING      DISTANCE = SQUARE ROOT [(X - X1)**2 + (Y - Y1)**2]
C
C      WHERE (X,Y) IS THE CENTROID OF ONE PARTICLE
C      AND (X1,Y1) IS THE CENTROID OF ANOTHER PARTICLE
C
C
C      P = DISTANCE BETWEEN PARTICLES (X-COORDINATES) SQUARED
C      Q = DISTANCE BETWEEN PARTICLES (Y-COORDINATES) SQUARED
C      NUM = NUMBER OF PARTICLES BEING ANALYZED
C      DIST = DISTANCE BETWEEN PARTICLES
C      MIND = EACH PARTICLE NEAREST NEIGHBOR DISTANCE FOR EACH
C      PARTICLE
C
C      DIMENSIONALIZE THE ARRAYS
C
C      REAL X(600),Y(600),MIND(600),DIST(600),P,Q
C
C      INITIALIZE THE VARIABLES AND ARRAYS
C
C      DO 160 L = 1, 600
C          P = 0.0
C          Q = 0.0
C          X(L) = 0.0
C          Y(L) = 0.0
C          DIST(L) = 0.0
C          MIND(L) = 0.0
160  CONTINUE
C
C      OPEN(UNIT=32,FILE='THS.DBI',STATUS='UNKNOWN')
C      OPEN(UNIT=33,FILE='THS.DBJ',STATUS='UNKNOWN')
C      OPEN(UNIT=60,FILE='AC0183.TXT',STATUS='UNKNOWN')
C
C      INPUT THE SIZE OF THE ARRAY (NUMBER OF PARTICLES)
C
C
C      PRINT *, ' '
C      PRINT *, 'HOW MANY PARTICLES ARE TO BE ANALYZED?'
C      PRINT *, ' '
C      READ *, NUM
C      PRINT *, 'THE NUMBER OF PARTICLES ANALYZED = ', NUM
C      WRITE(33,100) NUM
100  FORMAT(1X,'THE NUMBER OF PARTICLES ANALYZED = ',I5)
C
C      READ THE DATA FILES FROM IMAGE ANALYSIS
C
C      DO 130 K = 1, NUM

```



```

      READ(60,*) X(K), Y(K)
130  CONTINUE
C
C
C      FIND THE NEAREST NEIGHBOR DISTANCE
C
C
      WRITE(33,141)
141  FORMAT(/,1X,'THE NEAREST NEIGHBOR DISTANCE FOR PARTICLE NUMBER')
      DO 110 I = 1, NUM
          MIND(I) = 1000000.
          DO 120 J = 1, NUM
              P = (X(I)-X(J))**2
              Q = (Y(I)-Y(J))**2
              DIST(J) = SQRT(P+Q)
              IF(I.EQ.J) THEN
                  DIST(J) = 1000000.
              END IF
              IF(DIST(J).LT.MIND(I)) THEN
                  MIND(I) = DIST(J)
              END IF
          END DO
      END DO
120  CONTINUE
C
C
C      PRODUCE THE ARRAY OF NEAREST NEIGHBOR DISTANCES
C
C
      WRITE(33,140) I,MIND(I)
140  FORMAT(T15,I5,' = ',F13.4,' MICRONS')
      WRITE(32,170) MIND(I)
170  FORMAT(5X,F13.4)
110  CONTINUE
      END

```

APPENDIX B

HISTOGRAMS FOR MEAN ASPECT RATIOS AND MEAN FIRST NEAREST NEIGHBOR DISTANCES

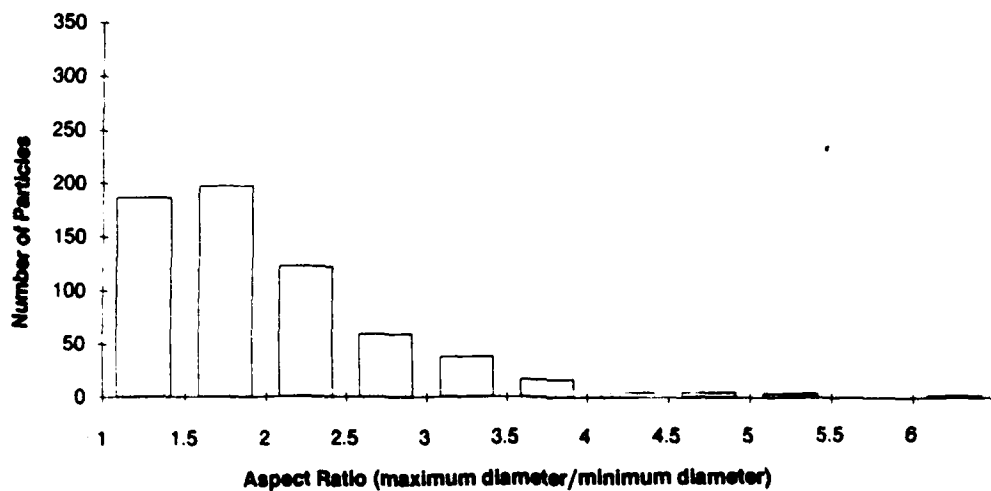


Figure 28: Particle Aspect Ratio Distribution for 7 inch (177.8mm) Diameter Casting. This data was obtained from micrographs such as that in Figure 5.

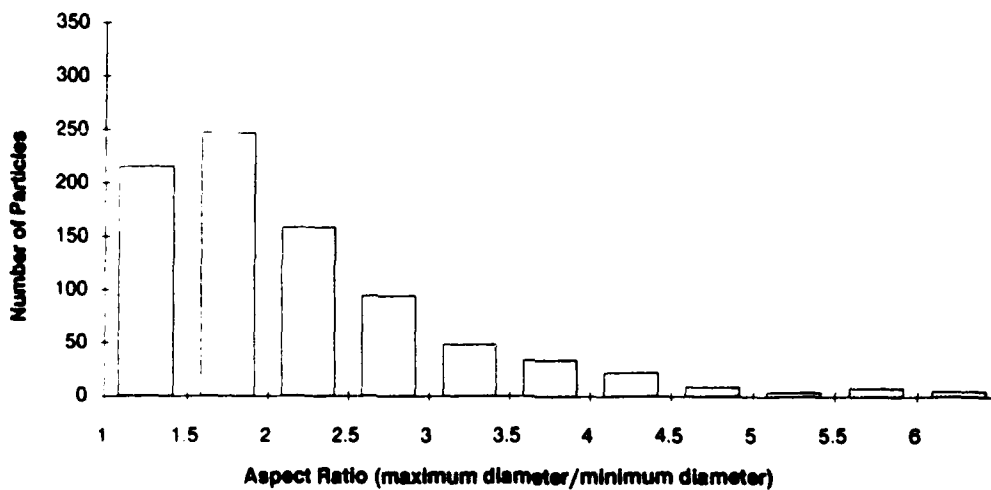


Figure 29: Particle Aspect Ratio Distribution for the Forged Condition. This data was obtained from micrographs such as that in Figure 6.

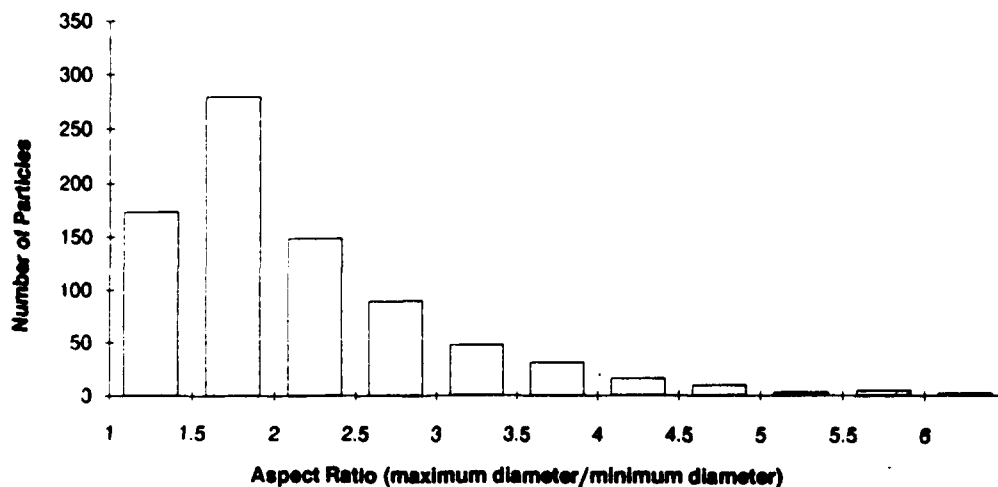


Figure 30: Particle Aspect Ratio Distribution for the Forged Condition. This data was obtained from micrographs such as that in Figure 7.

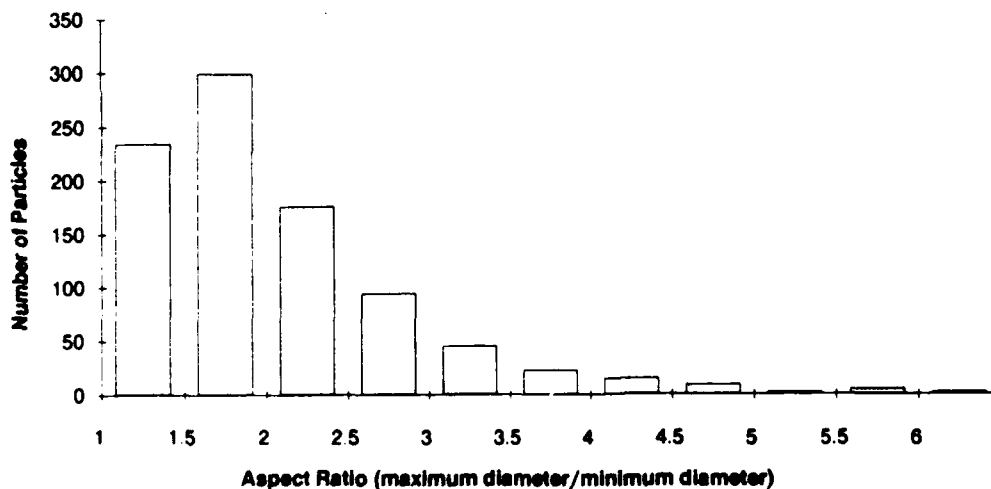


Figure 31: Particle Aspect Ratio Distribution for the Once Extruded to 2.5 inch (63.5mm) Diameter Bar. Sample in the as received condition as seen in the micrograph shown in Figure 8.

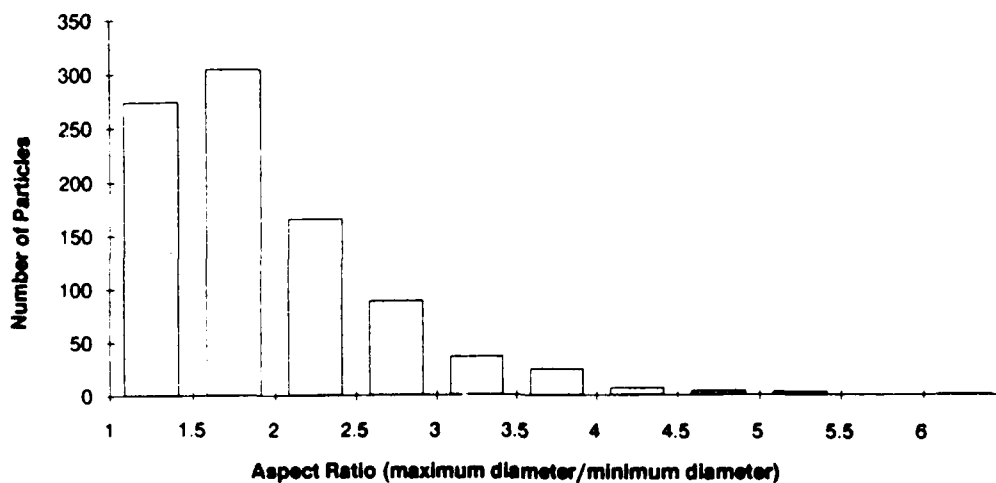


Figure 32: Particle Aspect Ratio Distribution for the Once Extruded to 2.5 inch (63.5mm) Diameter Bar. Sample has been solution heat treated for 70 minutes at 560° C. Data obtained from micrographs similar to those shown in Figure 12(b).

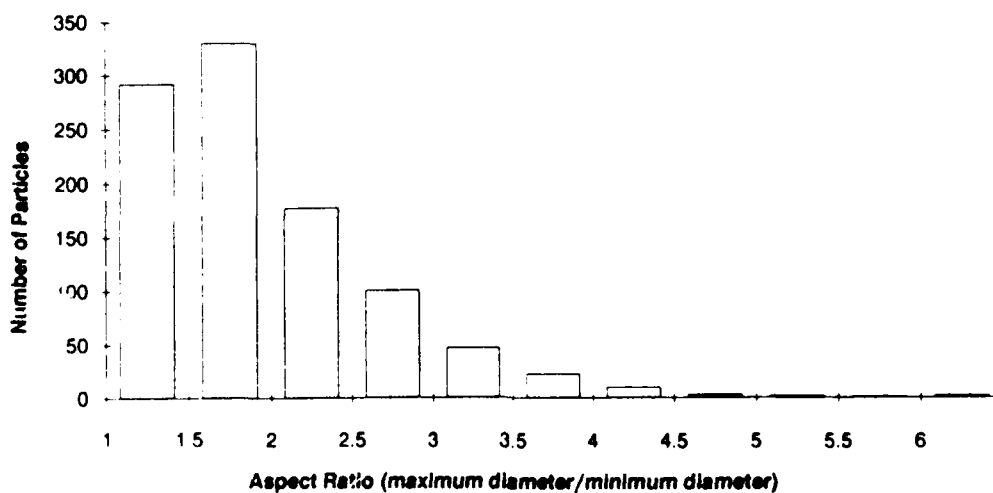


Figure 33: Particle Aspect Ratio Distribution for the Twice Extruded to 0.824 inch (20.9mm) Diameter Bar. Sample in the as received condition as seen in the micrograph shown in Figure 9.

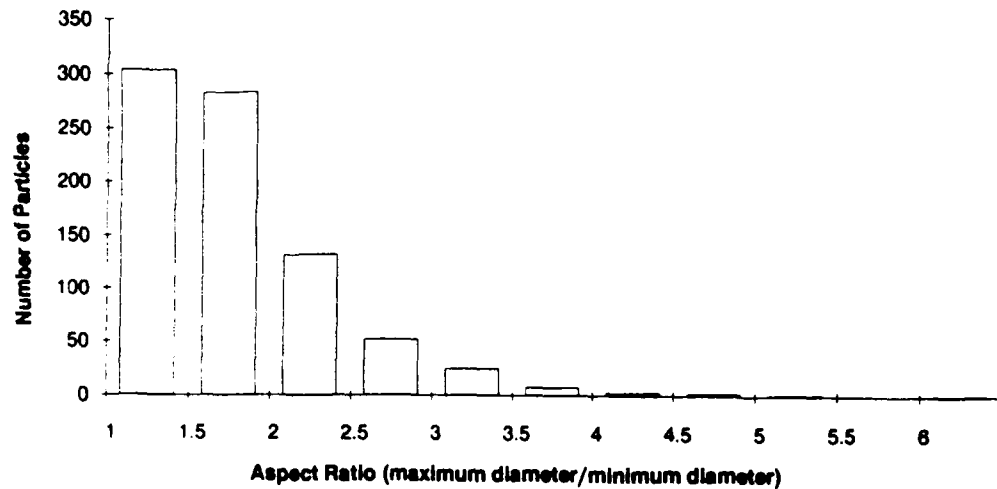


Figure 34: Particle Aspect Ratio Distribution for the Twice Extruded to 0.642 inch (16.3mm) Diameter Bar. Sample in the as received condition as seen in the micrograph shown in Figure 10.

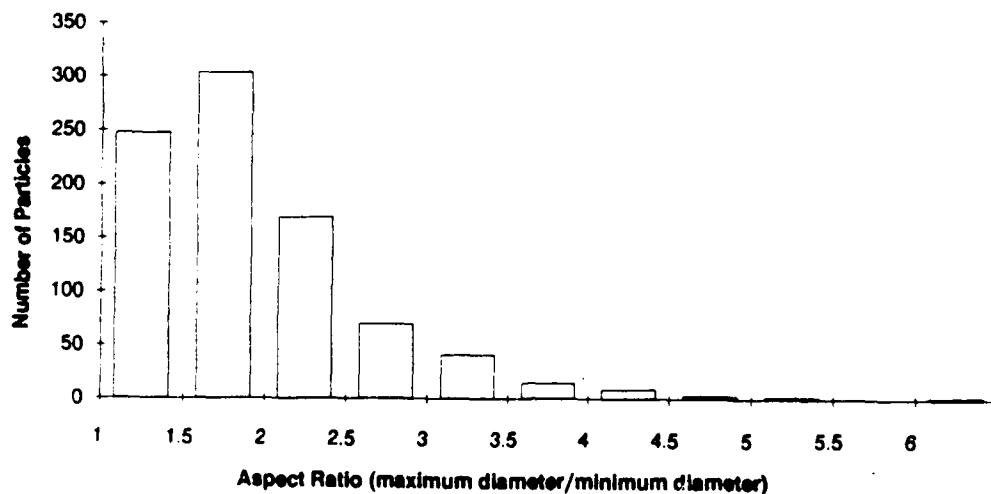


Figure 35: Particle Aspect Ratio Distribution for the Twice Extruded to 0.5 inch (12.7mm) Diameter Bar. Sample in the as received condition as seen in the micrograph shown in Figure 11.

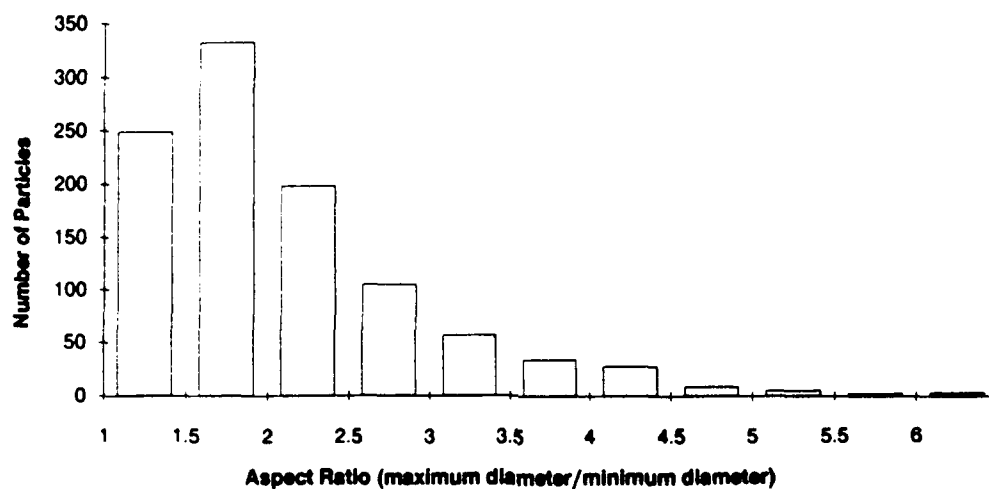


Figure 36: Particle Aspect Ratio Distribution for the Once Extruded to 0.5 inch (12.7mm) Diameter Bar. Sample has been solution heat treated for 70 minutes at 560° C. Data obtained from micrographs similar to those shown in Figure 13(b).

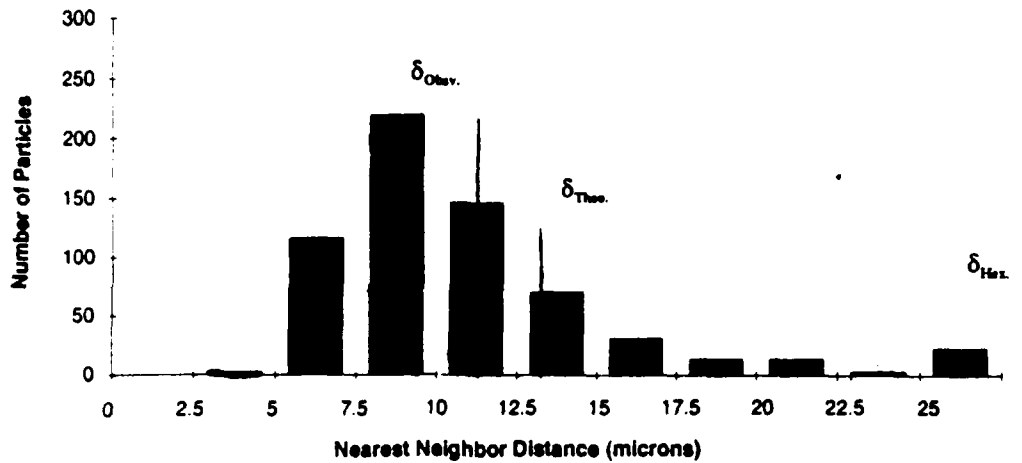


Figure 37: Particle First Nearest Neighbor Distance Distribution for 7 inch (177.8mm) Diameter Casting. This data was obtained from micrographs such as that in Figure 5.

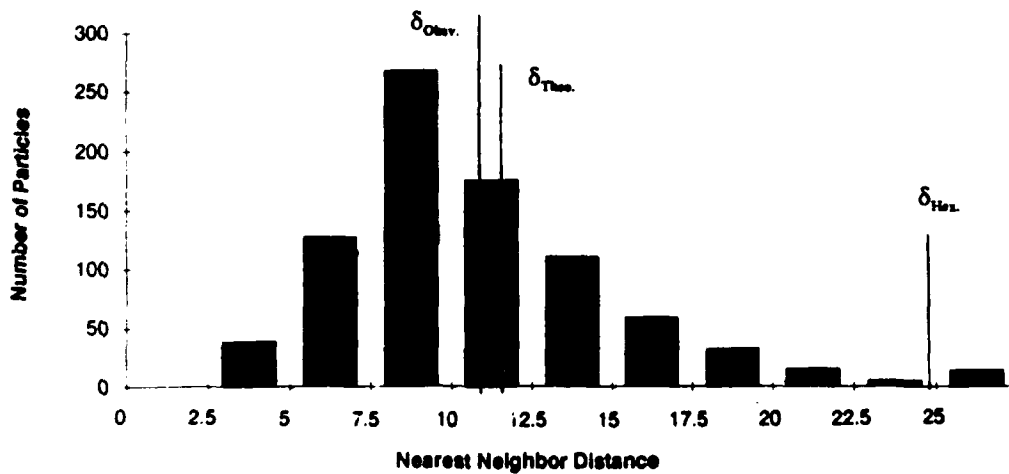


Figure 38: Particle First Nearest Neighbor Distance Distribution for the Forged Condition. This data was obtained from micrographs such as that in Figure 6.

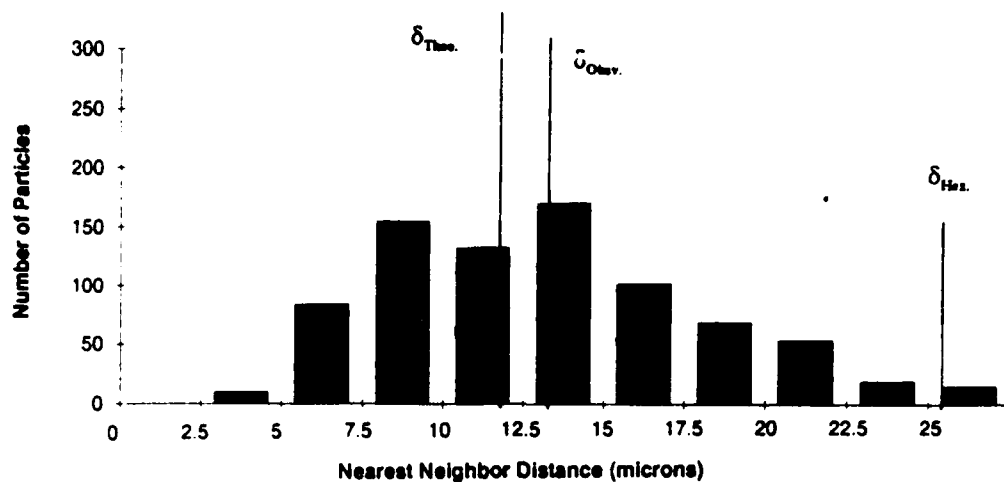


Figure 39: Particle First Nearest Neighbor Distance Distribution for the Rolled Condition. This data was obtained from micrographs such as that in Figure 7.

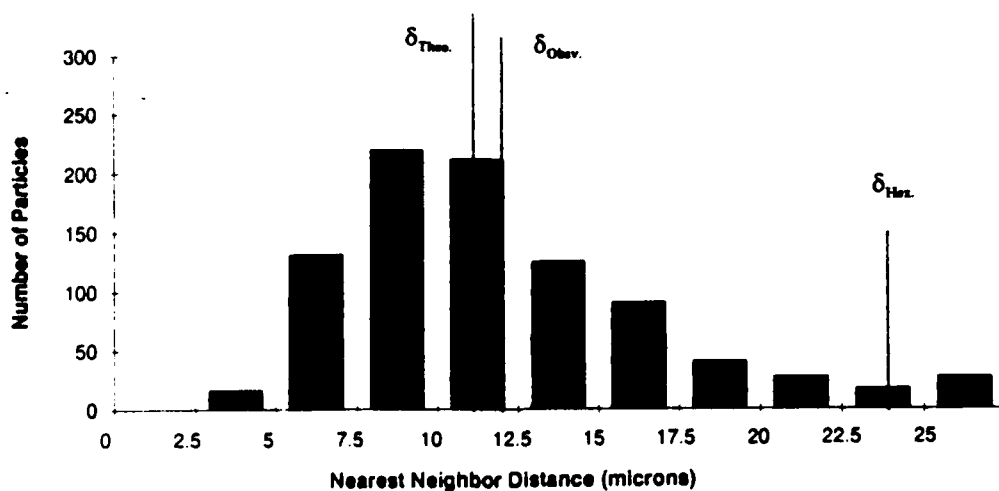


Figure 40: Particle First Nearest Neighbor Distance Distribution for the Once Extruded to 2.5 inch (63.5mm) Diameter Bar. Sample in the as received condition as seen in the micrograph shown in Figure 8.

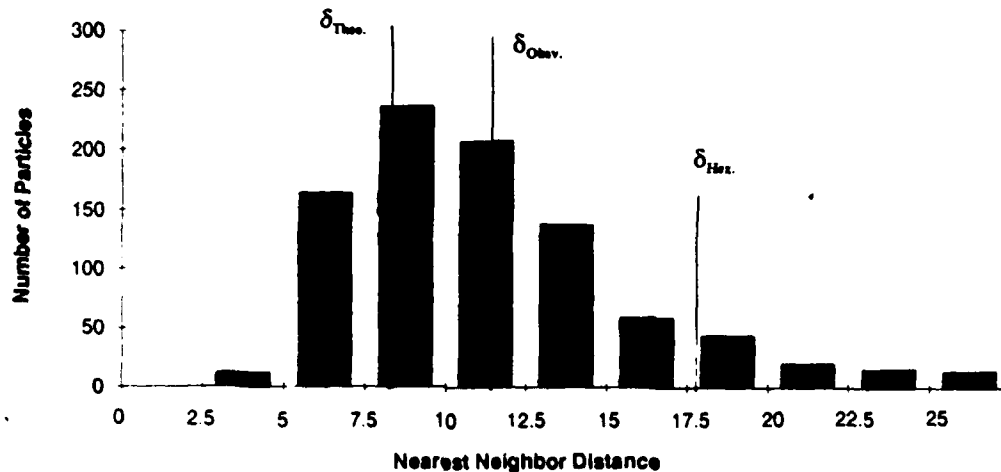


Figure 41: Particle First Nearest Neighbor Distance Distribution for the Once Extruded to 2.5 inch (63.5mm) Diameter Bar. Sample has been solution heat treated for 70 minutes at 560° C. Data obtained from micrographs similar to those shown in Figure 12 (b) .

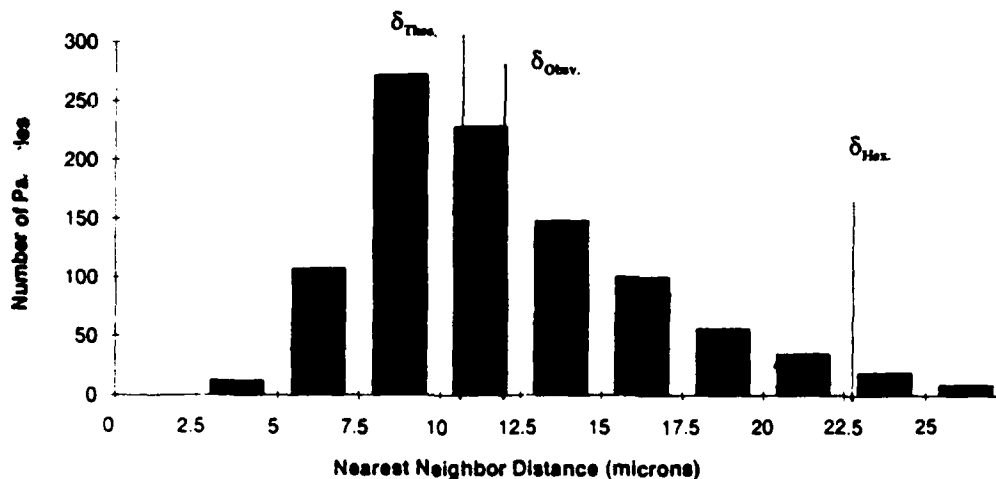


Figure 42: Particle First Nearest Neighbor Distance Distribution for the Twice Extruded to 0.824 inch (20.9mm) Diameter Bar. Sample in the as received condition as seen in the micrograph shown in Figure 9.

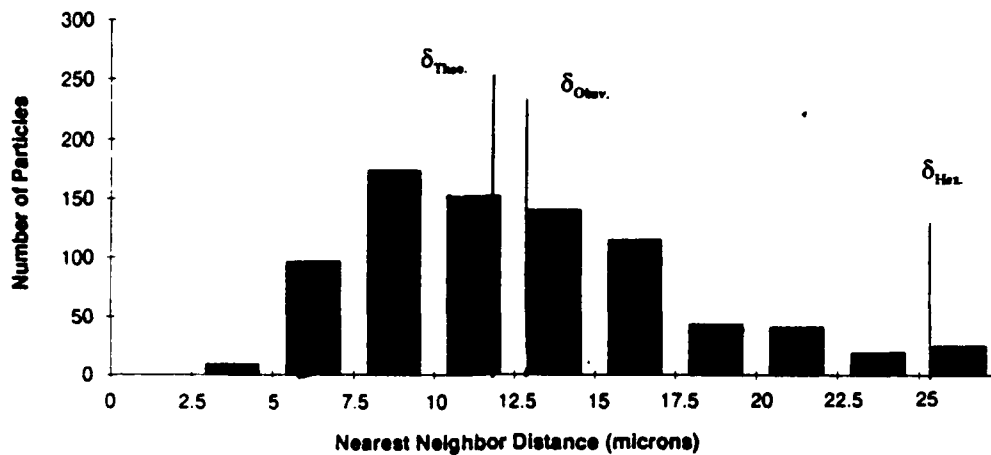


Figure 43: Particle First Nearest Neighbor Distance Distribution for the Twice Extruded to 0.642 inch (16.3mm) Diameter Bar. Sample in the as received condition as seen in the micrograph shown in Figure 10.

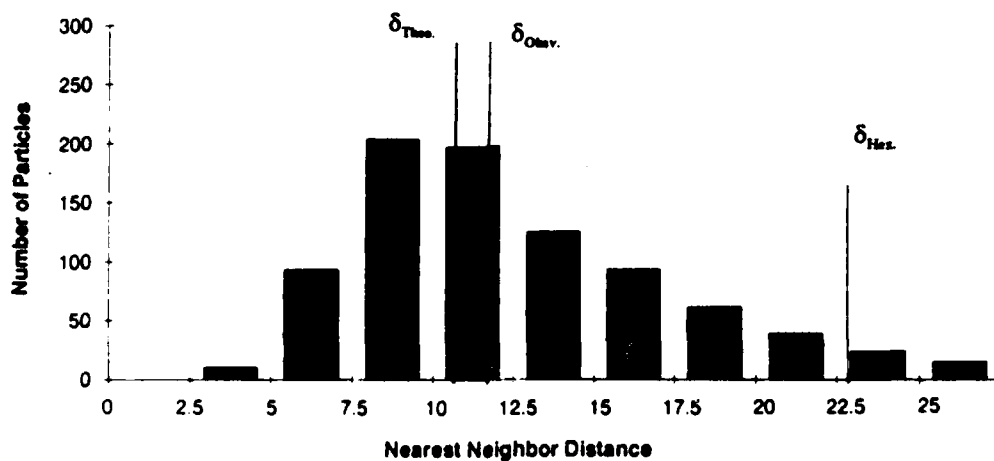


Figure 44: Particle First Nearest Neighbor Distance Distribution for the Twice Extruded to 0.5 inch (12.7mm) Diameter Bar. Sample in the as received condition as seen in the micrograph shown in Figure 11.

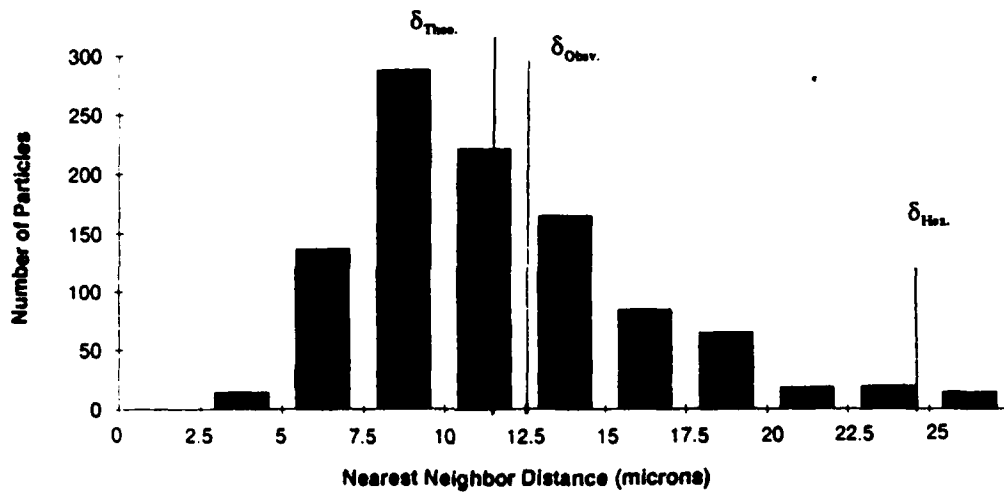


Figure 45: Particle First Nearest Neighbor Distance Distribution for the Twice Extruded to 0.5 inch (12.7mm) Diameter Bar. Sample has been solution heat treated for 70 minutes at 560° C. Data obtained from micrographs similar to those shown in Figure 13(b).

LIST OF REFERENCES

1. Callister, William D. Jr., *Materials Science and Engineering*, 2nd Edition, John Wiley & Sons, Inc., 1991.
2. Hoover, William R., "Recent Advances in Castable Metal Matrix Composites". *Fabrication of Particulates Reinforced Metal Composites*, Conference Proceedings, pp. 115-123, American Society for Metals (ASM) International, 1990.
3. McNelley, T. R., and Kalu, P. N., "The Effects of Thermomechanical Processing on the Ambient Temperature Properties and Aging Response of a 6061 Al-Al₂O₃ Composite", *Scripta Metallurgica et Materialia*, Vol. 25, pp. 1041-1046, May 1991.
4. Meyers, M. A. and Chawla, K. K., *Mechanical Metallurgy Principles and Applications*, p. 405, Prentice-Hall, Inc., 1984.
5. Jeffery, P. W. and Holcomb, S., "Extrusion of Particulate-Reinforced Aluminum Matrix Composites". *Fabrication of Particulates Reinforced Metal Composites*, Conference Proceedings, pp. 181-186, ASM International, 1990.
6. Eastwood, Jr., D. F., "The Effect of Thermomechanical Processing Parameters on the Ambient Behavior of 10% Volume 6061 Al-Alumina", Master's Thesis, Naval Postgraduate School, Monterey, California, March 1992.
7. Magill, M. D., "The Influence of Thermomechanical Processing Parameters on the Elevated Temperature Mechanical Behavior of a 6061 Aluminum-Alumina Metal Matrix Composite Materials", Master's Thesis, Naval Postgraduate School, Monterey, California, December 1990.
8. Macri, P. D., "Processing Microstructure and Elevated Temperature Mechanical Properties of a 6061 Aluminum-Alumina Metal Matrix Composite", Master's Thesis Naval Postgraduate School, Monterey, California, December 1990.
9. Manfredi, M. S., "Computer Simulation of Random and Non-Random Second Phase Particle Distributions for Both Constant and Varying Particle Size", Master's Thesis, Naval Postgraduate School, Monterey, California, September 1992.

10. Underwood, E. E., *Quantitative Stereology*, pp. 884-85, Addison-Wesley Publishing Company, Inc., 1970.
11. Humphreys, F. J., Basu, A., and Djazeb, M. R., "The Microstructure and Strength of Particulate Metal-Matrix Composites", UMIST, Conference Paper: Metal Matrix Composite-Processing, Microstructure and Properties, Roskilde, Denmark, 2-6 September 1991.
12. Nes, E., Ryum, N., and Hunderi, O., "On the Zener Drag", *Acta Metallurgica*, Vol. 33, No. 1, p. 22, 1985.
13. Hoyt, W. F., "The Effect of Thermomechanical Processing on Mechanical Properties of a Cast 6061 Al Metal Matrix Composite", Master's Thesis, Naval Postgraduate School, Monterey, California, September 1993.
14. Schauder, T. J., "The Effects of Thermomechanical/Processing Parameters on Elevated-Temperature Behavior of a 6061 Al- Al_2O_3 Metal Matrix Composite", Master's Thesis, Naval Postgraduate School, Monterey, California, March 1992.
15. Schaefer, T. A., "Thermomechanical Processing and Ambient Temperature Properties of A 6061 Aluminum 10 Volume Percent Alumina Metal Matrix Composite", Master's Thesis, Naval Postgraduate School, Monterey, California, March 1990.
16. Cronjager, L. and Meister, D., "Machining of Fiber and Particle Reinforced Aluminum", *CIRP Annales* 41, (1), 1992 pp. 63-66.
17. Land, C. T., "Machining Characteristics of Particulate-Reinforced Aluminum", *Fabrication of Particulates Reinforced Metal Composites*, Conference Proceedings, pp. 195-201, ASM International, 1990.
18. McNelley, T. R. and Kalu, P. N., "Thermomechanical Processing and Ductility Enhancement of a 6061 Al- Al_2O_3 Metal Matrix Composite", *Advanced Synthesis of Engineered Structural Materials*, Proceedings of the International Conference, August-September 1992.
19. *ASM Handbook*, Volume 4, Heat Treating, ASM International, p. 848, 1991.
20. *Metals Handbook*, 9th Edition, Volume 8, Metallography, Structures, and Phase Diagrams, ASM International, 1985.
21. *Metals Handbook*, 9th Edition, Volume 9, Metallography and Microstructures, ASM International, pp. 33-45, 1985.

22. Selvaduray, G., Hickman, R., Quinn, D., Richard, D., and Rowland, D., "Relationship Between Microstructure and Physical Properties of Al_2O_3 and SiC Reinforced Aluminum Alloys", *Interfaces in Metal Ceramics Composites Conference*, The Minerals, Metals, and Materials Society, 1990.

23. Humphreys, F. J., Miller, W. S., and Djazeb, M. R., "Microstructural Development During Thermomechanical Processing of Particulate Metal-Matrix Composites", *Materials Science and Technology*, Vol. 6, pp. 1157-1166, November 1990.

24. Miller, W. S. and Humphreys, F. J., "Strengthening Mechanisms in Particulate Metal-Matrix Composites", *Scripta Metallurgica et Materialia*, Vol. 25, pp. 35-38, 1991.

INITIAL DISTRIBUTION LIST

	No. Copies
1. Defense Technical Information Center Cameron Station Alexandria VA 22304-6145	2
2. Library, Code 052 Naval Postgraduate School Monterey CA 93943-5002	2
3. DURALCAN-USA c/o William Dixon 10505 Roselle Street San Diego, CA 92121	2
4. Chairman, Code ME/Kk Mechanical Engineering Department Naval Postgraduate School Monterey, CA 93943-5100	1
5. Professor T. McNelley, Code ME/Mc Mechanical Engineering Department Naval Postgraduate School Monterey, Ca 93943-5100	5
6. Naval Engineering Curricular Officer, Code 34 Naval Postgraduate School Monterey, CA 93943-5100	1
7. LT Fredric W. Longenecker Shore Intermediate Maintenance Activity Box 141 Pearl Harbor, HI 96860	2